SAPIENZA
UNIVERSITÀ DI ROMA

Faculty of Pharmacology and Medicine

Department of Molecular Medicine

PhD course in Molecular Medicine

Characterization of MEN1309/OBT076, a new antibody conjugated to the DM4 maytansinoide toxin

Faculty Supervisor: Prof. Gianluca Canettieri

PhD candidate: Giuseppe Merlino

Co-supervisors: Dott. Mario Bigioni

TABLE OF CONTENTS

1. Abstract

CD205 is a type I transmembrane glycoprotein, member of C-type lectin receptor family. Analysis by mass spectrometry revealed that CD205 antigen was robustly expressed and highly prevalent in a variety of solid malignancies of different histotypes. Immunohistochemistry (IHC) confirmed the increased expression of CD205 antigen in pancreatic, bladder and triple negative breast cancer (TNBC) malignancies compared to corresponding normal tissues. Using immunofluorescence microscopy, rapid internalization of the CD205 antigen was observed. These results supported the development of MEN1309/OBT076, a fully human CD205-targeting monoclonal antibody conjugated to DM4, a potent maytansinoid derivate, via a cleavable N-succinimidyl-4-(2-pyridyldithio) butanoate linker. MEN1309/OBT076 was characterized in vitro for target binding affinity, mechanism of action (MoA) and cytotoxic activity against a panel of cancer cell lines demonstrating selective and potent cytotoxic effects against tumor cells with strong and low to moderate CD205 antigen expression. In addition, MEN1309/OBT076 showed potent antitumor activity resulting in durable responses and complete tumor regressions in many xenografts of TNBC, pancreatic, bladder cancer cell-lines as well as in patient-derived xenograft (PDX) models. Finally, the pharmacokinetics (PK) and pharmacodynamics (PD) profile of MEN1309/OBT076 was characterized in a mouse model harboring a pancreatic tumor. Overall, these data demonstrate that MEN1309/OBT076 is a novel and selective antibody-drug conjugate (ADC) with potent activity against CD205 antigen positive tumors. These data supported the clinical development of MEN1309/OBT076 in the phase I of “SHUTTLE” clinical trial, currently ongoing.

2. Introduction

2.1 Targeted Therapy: Antibody Drug Conjugates (ADC)

The targeted strategy was historically articulated by the remarkable German scientist, Paul Ehrlich, more than 100 years ago, indeed he coined the term “magic bullets” to describe such molecules [1, 2].

‘Targeted therapy’ employs direct and indirect approaches to exploit their therapeutic potential. The former are directed against tumor-associated or tumor-specific proteins to alter their oncogenic signalling either, by monoclonal antibodies (mAbs) binding to the relevant antigens or by small molecules, low-molecular weight drugs that interfere with these proteins (molecular targeting). The indirect approaches rely on tumor-associated proteins, expressed on the cell surface, serving as target device for fusion proteins containing different kinds of cytotoxic molecules [3].

ADCs belong to the indirect approach strategy and represent a promising therapeutic modality for oncology indications.

This new class of therapeutic agents consists of three components: i) the antibody, designed to recognize a specific tumor-associated antigen, ii) the chemical linker, designed to release the cytotoxic agent within the cell, and iii) the payload, usually a small molecular weight with the most powerful cytotoxin (Figure 1). Their synergy allows a targeted delivery of toxic drugs to cancer cells while sparing healthy cells [4].

The complex, after the antigen-antibody binding, is internalized inside the cells and the payload is releasedv by lysosomes allowing the killing of the cells.

Considering the limited clinical efficacy and the systemic toxicity of some of the currently available cytotoxic drugs, ADCs have the potential to wide their therapeutic window, by lowering the minimum effective dose (MED) and increasing the maximum tolerated dose (MTD)[5].

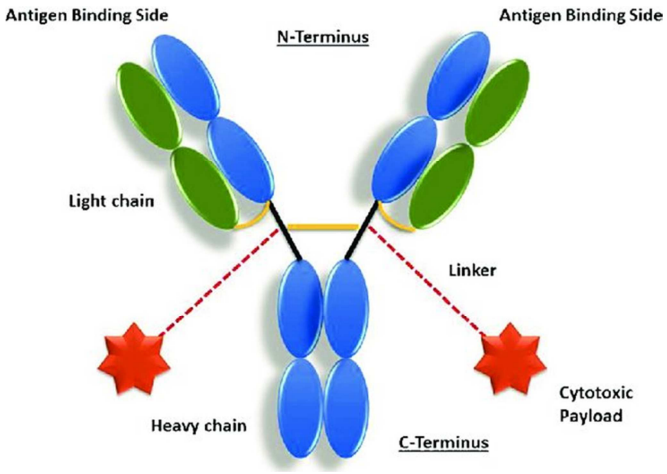

Figure 1. Schematic representation of an ADC structure. The antibody is comprised of heavy (blue) and light (green) chains, and contains antigen-binding sites at the N-terminus engineered to recognize antigens associated with a tumor cell. The cytotoxic payloads are connected via linkers to the antibody, with the example shown having two payloads attached via cysteine residues in the hinge region

2.1.1 Target and Antibody

The first step in the ADC development is represented by the selection of the tumor antigen, which should be ideally homogenously overexpressed on the surface of the tumor cells and with a limited or absent expression on the cell surface of healthy cells in order to guarantee the site-specific targeting and delivery of cytotoxic payloads [6]. Different technical approaches such as immunohistochemistry (IHC), flow cytometry, tissue microarray, reverse transcription polymerase chain reaction (TR-PCR), and messenger RNA (mRNA) profiling, are commonly used to evaluate the expression of the

target antigen in patient-derived tumor tissue samples [7]. In addition, the ability of the antibody-antigen complex to internalize into the cell to enable the delivery of the linked payload, called receptor-mediated endocytosis, [5] is another important factor that is dependent on the nature of the antigen.

The next step, upon confirmation of the target antigen overexpression, is the generation of monoclonal antibodies by Hybrodoma Technology [8]. Upon the mAbs generation, two additional characteristics need to be carefully evaluated in order to select a potential ADC candidate: the binding affinity and the tumor penetrating ability. The optimal biding affinity for an ADC should have a K_d < 10nM, in order to ensure a good tumor localization, although the balance between internalization and disassociation rates of the antigen-antibody (Ab-Ag) complexes governs effective delivery of the payload to the tumor space [6]. Shedding of tumor the antigen from human tissues and the presence of the circulating antigen in perpheral blood can alter the potency and the pharmacokinetics of the ADC, making this information relevant for the identification of the proper antigen to be targeted [9].

The most used immunoglobulin for ADC development is the IgG isotype, specifically IgG1, due to its ability to trigger immune-mediated effector functions too. The most well known Fragment crystallizable (Fc)-mediated antibody effector functions are antibody-dependent cellular cytotoxicity (ADCC), through the binding of its Fc portion to the Fcɣ receptors on the immune cell membranes, and the complement-dependent cytotoxicity (CDC), through the binding of its Fc portion to C1q protein complex [10]. On the contrary IgG2 and IgG4 are typically deficient in their effector functions [11], while IgG3 isotypes are not used as therapeutics due to a significantly faster clearance rate [12].

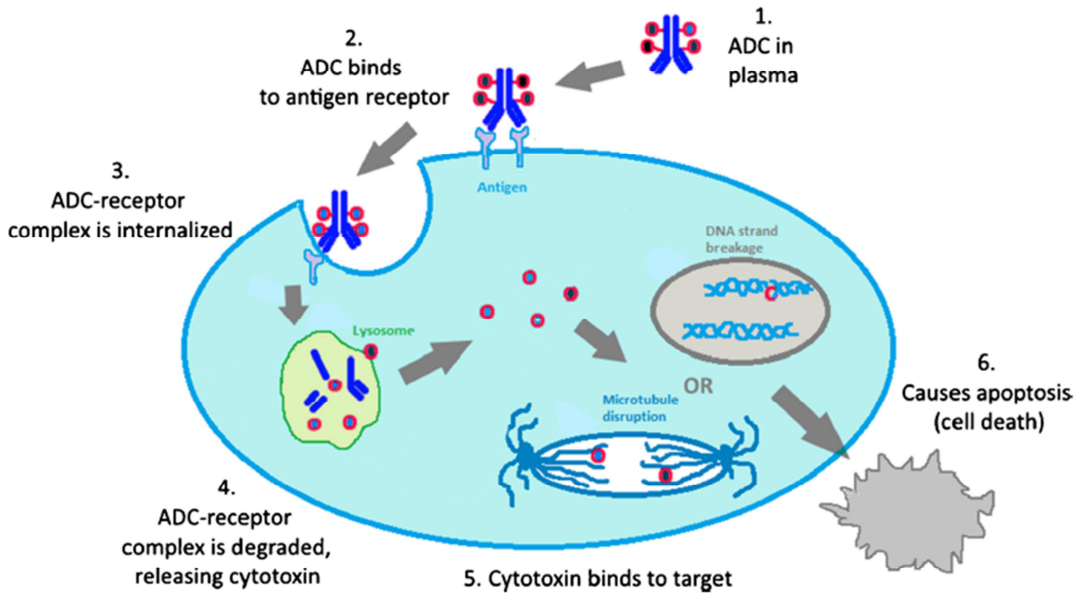

Figure 2. Mechanism of action of an ADC. Step 1: ADC is prepared and released into blood stream. Step 2: The mAB component binds the tumor antigen expressed on the cell surface. Step 3: The ADC-antigen/receptor complex undergoes receptor-mediated endocytosis, getting internalized inside the tumor cell. Step 4: Lysosomes fuse with late endosomes allowing the release of the toxin. Step 5: Cytotoxin interferes with critical cell machinery (microtubule assembling). Step 6: The tumor cell dies due to apoptosis.

2.1.2 Linker

One of the main challenges in developing ADCs is to select an appropriate linker and the chemistry used to bind the linker to the antibody. Indeed, the sites of conjugation and the selection of the most appropriate linker technologies play crucial roles in: 1) ADC stability in circulation (lack of linker stability causes premature release of the payload and undesired damages to the non-targeted healthy cells, which can lead to systemic toxicity and adverse effects), 2) pharmacokinetics properties [6], 3) water solubility in order to avoid formation of inactive ADC aggregates [13] and 4) ability to overcome the multidrug resistant mechanisms [14].

Based on the payload release mechanism, linkers are generally divided into cleavable and non-cleavable.

The principal advantage of the cleavable linker is that the ADC is metabolized in order to release the uncharged and membrane permeable toxin after ADC internalization in positive-antigen cancer cells. Thus the use of the clevable linker allows the killing of adjacent antigen-negative cells by the membrane permeable toxin[15]. This phenomenon is called by-stender effect and it can be useful for treating tumors with heterogeneous antigen expression [16]. On the other hand, this effect might increase the off-target toxicity. An alternative mechanism based on non-internalization of antigen-antibody complex has been also described. In this case, the payload release occurs in the extracellular tumor microenvironment [17].

Cleavable linkers may include chemically labile (pH dependent and disulphide) and enzyme-labile (peptide-based) linkers. These linkers are cleaved only after internalization by the target cell with subsequent lysosomal degradation releasing free drug [17].

- *Acid-labile or pH-dependent linkers* are designed to be stable at the relatively neutral pH of blood but are hydrolysed when in an acidic environment (pH 5) such as in lysosomes or endosomes. Although degradation of the acid-labile linker in the acidic lysosome is the major degradation pathway for drug release, studies have shown that this may also happen extracellularly [16, 17].

- *Disulphide linkers* use a direct covalent bond between sulphide groups belonging to the drug and linker. Two linkers, N-succinimidyl-4-(2-pyridyldithio)pentanoate (SPP) and N-succinimidyl-4-(2-pyridyldithio)butanoate (SPDB), which contain one or two methyl groups adjacent to the disulphide bond, respectively, resulting in

increasing steric hindrance, have been used for ADCs. The more sterically hindered SPDB linker showed superior activity compared with the SPP linker (19), and in some cases these cleavable linkers result in more potent ADCs than their non-cleavable linker counterparts [18]. Although ADCs using clevable linkers can cause bystander killing, it is believed that internalisation, reduction of the disulphide bond, and further modification to the drug within the target cells are required for modifying the potency of the drug once released from the cell to cause the bystander killing [16].

The recent 'traceless' technology uses a direct, unhindered disulphide bond between a drug and an antibody or a small immune protein (SIP). The resulting drug conjugates do not require internalisation by the target cell because the drug is released upon reduction or hydrolysis of the disulphide bond within the tumor microenvironment [19].

- *Enzyme-labile (peptide-based) linkers* are composed of a dipeptide linker, which are cleaved preferentially by the lysosomal protease, cathepsin B and they are more stable in both human and mouse plasma than the pH dependent hydrazone linker [17]. Cathepsin B has a relatively broad scope of substrate, but it preferentially recognizes certain sequences such as phenylalanine-lysine (Phe-Lys) and valine-citrulline (Val-Cit) and cleaves a peptide bond on the C-terminal side of such sequences aid the release of the payload [20].

Another interesting observation was the different metabolite profiles for different linker types. With the cleavable linkers releasing cytotoxic drug, and the non-cleavable linkers releasing, the drug attached to an amino acid: e.g., maytansinoid ADCs with the non-cleavable linker MCC-DM1 produced only lysine-MCC-DM1 whereas ADCs with cleavable

linkers SPP-DM1 and SPDB-DM4 produced multiple metabolites including lysine- SPP-DM1, DM1, S-methyl-DM1, S-methyl-DM1 sulfoxide and S-methyl-DM1-sulfone (for mAb-SPP-DM1), and lysine- SPDB-DM4, DM4, S-methyl-DM4, S-methyl-DM4-sulfoxide and S-methyl-DM4-sulfone (for mAB-SPDB-DM4) [21]. Some of these metabolites could also enhance anti-tumor activity via bystander killing mechanisms where the cytotoxic agent released in one cell diffuses to neighbouring cells and exerts its effect [22].

Non-cleavable linkers consist of stable bonds that are resistant to proteolytic degradation, ensuring greater stability than the cleavable linkers. Non-cleavable linkers rely on complete degradation of the antibody component of ADC by cytosolic and lysosomal proteases, which eventually release a payload molecule linked to an amino acid residue derived from the degraded antibody. As such, when coupled with a non-cleavable linker, the payload structure must be carefully selected and designed so that payload can exert comparable or even better anti-tumor potency in such a modified form. For that purpose, it may be necessary to examine Pharmacokinetic/Pharmacodynamic (PK/PD) and toxicity profiles of all possible metabolites of ADCs with non-cleavable linkers [20]. A successful example of ADC using a non-cleavable linker is the humanized anti-HER2 antibody-maytansine conjugate trastuzumab emtansine (T-DM1, or Kadcyla®).

2.1.3 Payload

To create an efficacious ADC, it is imperative to have a potent cytotoxic payload. The cytotoxic payloads used so far for ADCs development can be divided in two different classes, based on their mechanism of action: DNA damaging agents and tubulin polymerization inhibitors.

DNA damaging agents

Calicheamicins is a highly potent enedyne antitumor antibiotic, originally isolated from the actinomycete *Micromonospora echinospora;* it binds to the minor groove of DNA and cleaves double-stranded DNA in a site specific manner [23]. This molecule is very hydrophobic and only few molecules per immunoglobulin can be conjugated to avoid high level of aggregates protein. It is less dependent on cell cycle progression making it potentially useful against cancer stem cells who have lower rates of proliferation [24] .

Duocarmycins, such as duocarmycin A, are a family of naturally occurring antibacterial agents initially isolated from the bacterial cultures of Streptomyces zelensis [25]. They are DNA minor groove binders and exert their high potency through a sequence-specific alkylation of DNA, preferring the N3 position of DNA strands [6].

Pyrrolobenzodiazepine (PBPs), are based on naturally occurring antitumor antibiotics that bind to the DNA minor groove in a sequence-specific manner. They covalently bind to a particular sequence in DNA minor groove and form an amine bond in-between C11 of PBD and N2 of guanine bases [26]. Although they do not disrupt the DNA structure considerably, formation of DNA-PBD adduct impedes key DNA functions like transcription and translation [27]. In addition, generally, they are not a substrate for MDR1 and thus they can retain activity in MDR1 positive tumor [28].

Camptothecin (CPT), a pentacyclic quinolone-based plant alkaloid, was first isolated from the deciduous Asian tree *Camptotheca acuminata* [29]. CPT was shown to possess potent antitumor activity by selectively inhibiting DNA topoisomerase I, thus effectively stalling DNA replication in S-phase arrest and resulting in the apoptotic cell death of tumor cells [30]. Due to its chemical-physical features, such as poor water solubility, its clinical

development was prevented, but its analogue, SN38, was often used in the clinical practice. SN38, the active metabolite of the anticancer prodrug irinotecan, acts via inhibition of DNA topoisomerase 1. SN38 is approximately three orders of magnitude more potent than irinotecan and cannot be administrated directly to patients because of its toxicity and poor solubility [12].

Tubulin polymerization agents

Tubulin polymerization inhibitors (auristatins and maytansinoids) are widely employed as cytotoxic payloads [31].

Auristatins: they are water-soluble synthetic analogs of a marine natural product (dolastatin 10) isolated form the extract of a sea hare, *Dolabella auricularia*. They share the same tubulin-binding site as vinca alkaloids and inhibit tubulin polymerization and tubulin-dependent GTP hydrolysis that causes cell cycle arrest in the G2/M phase, eventually leading to cell death [32]. Two auristatin derivatives (MMAE and MMAF), which are currently being used as payloads in several ADCs by linking to the cysteine residues of the mAb [6]. MMAE can penetrate the cell membrane, and as a result it can prompt bystander killing where it diffuses through nearby cells independent of antigen expression, by contrast, MMAF is impermeable to cell membrane [33]. This is because MMAF is more hydrophilic, less potent, and less toxic than MMAE.

Maytansinoids: the second largest class of payload used in ADCs in clinical trials are those based on maytansinoids (DM1 and DM4). DM1 and DM4 are derived from maytansine, which is a natural benzoansamacrolide product isolated from the bark of the African shrub *Maytenus ovatus* [34]. Maytansine binds to the same site on tubulin as the vinca

alkaloids, with similar in vitro inhibition constants, but it is a more-potent cyto-toxin. It failed as an anticancer agent in clinical trials because of systemic toxicity [35]. However, it has excellent stability and acceptable solubility in aqueous solutions for the use as an ADC building block.

2.1.4 Drug Antibody Ratio (DAR) and Conjugation step

Drug Antibody Ratio (DAR) is defined as the number of drug molecules per mAb. DAR plays a key role in developing ADCs, as it determines the dose needed to produce the desired effect in patients. There are a limited number of drug molecules that can be efficiently delivered to the target site and in addition, drug loading significantly contributes to the pharmacokinetics profile of ADC. If fewer drug molecules are conjugated per mAb, the ADC system will not be clinically effective. On the other hand, conjugating too many drug molecules per mAb will make the ADC unstable, toxic and may lead to aggregation and immunogenic reactions [36, 37]. Normally, ADCs contain different species with differing DAR values and every species has its own distinct pharmacokinetics. ADCs with heavily loaded drugs are more rapidly cleared from the system. In general, an average DAR of 3–4 is used to achieve optimum effect in ADCs, depending upon potency of the payload [38, 39].

Several strategies have been employed for cross-linking the antibody to the payload by a linker using solvent reachable reactive amino acids with nucleophilic groups in antibody side chains. Side chain cysteine (SH group) and lysine (NH2 group) have been extensively used for conjugation. The main problem with these conventional conjugation methods is the heterogeneous nature of the final products with different DAR values and un-

conjugated antibody production [38]. In addition, the conjugation strategy must not alter any key blocs of the antibody that are responsible for its binding to the target antigen. Moreover, un-conjugated antibodies occupy the target antigen, thus competing with the ADC for internalization into antigen-postive cells.

The location of the linker on the antibody structure could also impact ADC functions. If the linker is conjugated in the Fragment antigen-binding (Fab) region of the antibody this may interfere with or completely impair antigen recognition and the targeting of the ADC to tumors. Conjugation at or near the Fc regions, may also hinder binding to the neonatal Fc receptor (FcRn) and/or Fc receptors on immune effector cells, or alter antibody folding and structure [40].

Engineering of the conjugation site, with a site-specific conjugation site may lead to a more homogenous product with defined and uniform drug stoichiometry. The principal site-conjugation technologies are: Engineering of Side Chain Cysteine Residues (ThioMab) [41], the incorporation of non-natural amino acids (unAA) [42] and the enzymatic site-specific conjugation process [43].

2.1.5 Pharmacokinetics considerations

An important question in the development of ADCs is to define the exposure-response relationship for both efficacy and safety.

Understanding the pharmacokinetics of the ADC, exposure at the site of action and also the drivers of efficacy and toxicity are key topics, important to address, in order to enable the design of an efficacious ADC characterized by an appropriate therapeutic window.

The theoretical ADC elimination pathways include the deconjugation, degradation/catabolism through non-specific or target-mediated proteolysis [9]. These processes can happen in the circulation and/or intracellularly, depending on the ADC feature components.

Deconjugation of the ADC leads to the formation of unconjugated antibody and unconjugated drug, while catabolism of the ADC leads to the formation of antibody fragments and/or drug containing catabolites. The unconjugated antibody or antibody fragments can further undergo proteolysis to generate/release amino acids. The cytotoxic drug and drug related catabolites can undergo metabolism via Cytochrome P450 (CYP) or non-CYP enzymes or be transported by transporters like P-glycoprotein and get excreted via the biliary or renal route [44].

The overall PK characteristics of an ADC such as slow clearance, long half-life and limited tissue distribution are driven by its antibody component. In addition to the antibody component, there are additional elimination mechanisms related to its linker and drug component.

The relatively long life of an ADC compared to a small molecule is due to recycling via Neonatal Fc Receptor (FcRn), which protects it from catabolism in the lysosomes. Similarly to the naked antibodies, the ADC can be taken up into cells specifically via receptor mediated endocytosis (target dependent mechanism) or non-specifically via pinocytosis (target-independent mechanism). FcRn-bound ADC can be recycled back to the cell surface and released back into circulation while ADC that is not bound to FcRn undergoes proteolytic degradation in the lysosome [44].

Tumor and antigen accessibility is a critical factor and often a major hurdle for effective antibody drug delivery. It has been reported that only 0.001% to 0.01% of an injected unmodified antibody, and by analogy, an ADC, localizes to tumors in patients [45]. Indeed, the tissue distribution of an ADC, is limited with the initial distribution in the vascular space followed by slow diffusion across vascular endothelial cells into tissues, where it will bind the target antigen on tumor cell surfaces. This restricted uptake is further compromised by the fact that tumors often lack functional lymphatics vessels [46] which can lead to increased levels of interstitial fluid pressure (IFP) [47]. An increase in IFP is likely to reduce convection and thereby inhibit the uptake of antibodies [48]. Small tumors (or micro metastases) on the other hand, tend to exhibit a more uniform circulatory system and lower IFP and, as a result, ADC delivery should be more efficient under these conditions.

Other factors that impact PK and tissue distribution of an ADC that are similar to nacked antibodies are the presence of soluble and/or shed antigen in circulation that can form immune complexes upon binding to the ADC [49]. The complexed might increase the immunogenicity potential of the ADC (i.e., the formation of anti-therapeutic antibodies, ATAs) leading to ADC clearance and decrease exposure that may reducece the ADC activity [50]. In addition, the immunogenicity can impact on the tolerability profile of the ADC.

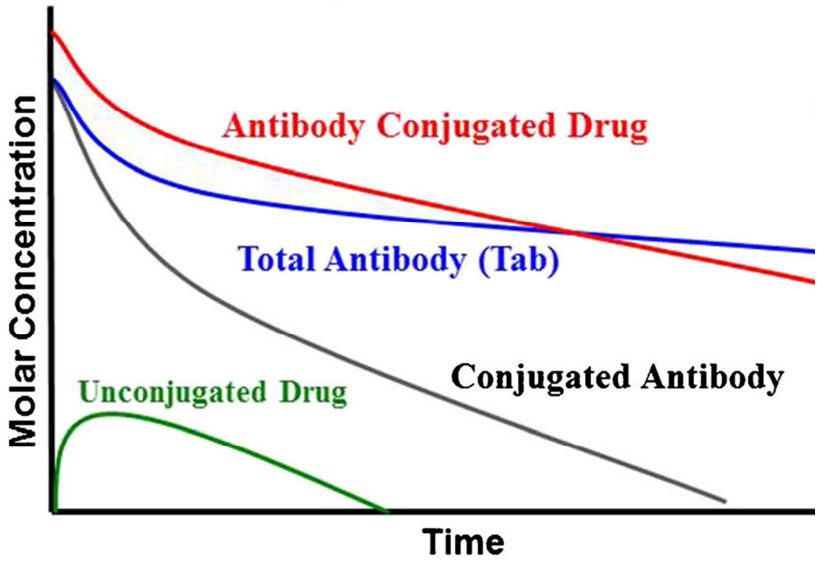

Figure 3. Schematic Pharmacokinetics profile of a classical ADC. The red line represents the serum concentration of the ADC; the blue line represents the total antibody (conjugated and not conjugated); the black line represents the drug conjugated with the antibody; the green line represents the unconjugated drug.

2.1.6 FDA approved ADCs and current clinical trials

Today, a number of different ADC-based treatment options are available for both haematological malignancies and solid tumors. These options have dramatically increased the efficacy of treatment and are now considered among the most promising strategies used for targeted therapy of patients with a variety of malignancies.

There are four ADCs currently approved and commercially available in the United States (US) and European Union (EU). The first ADC, gemtuzumab ozogamicin (Mylotarg™, previously known as CMA-676; Wyeth Pharmaceuticals, a subsidiary of Pfizer), was approved in 2001 for the treatment of acute myelogenous leukemia (AML), but it was withdrawn from the market in June 2010 due to a serious and potentially fatal liver condition. Gemtuzumab ozogamicin was resubmitted for approval with a fractionated

dosing regimen and was recently (September 2017) approved by the US Food and Drug Administration (FDA) for the treatment of AML patients.

Until the summer of 2017, brentuximab vedotin (Adcetris®; Seattle Genetics) and ado-trastuzumab entansine (Kadcyla®; Genetech/Roche) were the only two commercially available ADCs indicated for the treatment of relapsed Hodgkin lymphoma (HL) and anaplastic large cell lymphoma (ALCL) and treatment of HER2-positive metastatic breast cancer (mBC) in patients who have been treated previously with trastuzumab and a taxane (paclitaxel or docetaxel), respectively. Then, on August, 2017, the FDA approved inotuzumab ozogamicin (Besponsa™, Wyeth Pharmaceuticals Inc., a subsidiary of Pfizer Inc.) for the treatment of adults with relapsed or refractory B-cell precursor acute lymphoblastic leukemia (ALL).

Nowadays, there are nearly 175 investigational ADCs in development, from early discovery to pivotal, late stage, clinical phase III studies.

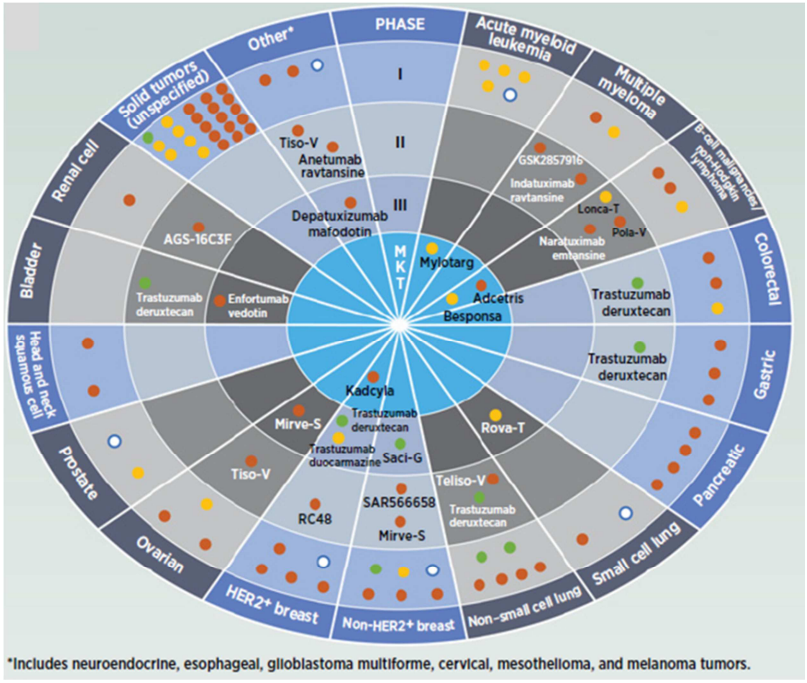

Figure 4. ADCs in clinical development.The rounds represent the clinical phase, the slides represent the tumor type in which the ADCs are developed, the orange dots represent the ADCs conjugated with the microtubule inhibitor

payload, the green dots represent the ADCs conjugated with the topoisomerase inhibitor payload, the yellow dots represent the ADCs conjugated with DNA-damaging payload, the white dots represent the ADCs conjugated with an unknown payload.

Gemtuzumab Ozogamicin (Mylotarg™)

The first ADC to receive marketing approval from the FDA in 2000 was gemtuzumab ozogamicin (Mylotarg™). Gemtuzumab ozogamicin is a humanized IgG4 anti-CD33 monoclonal antibody covalently linked to the antitumor antibiotic calicheamicin by an acid-labile linker (bifunctional linker, 4-(4-acetylphenoxy) butanoic acid). It does not elicit antibody effector functions. Today, it is indicated for the treatment of newly-diagnosed CD33-positive acute myeloid leukemia in adults and the treatment of relapsed or refractory CD33-positive AML in adults and in pediatric patients 2 years and older. Gemtuzumab ozogamicin binds to the CD33 antigen expressed on the surface of leukemic blasts, normal myeloid cells, and leukemic clonogenic precursors [51]. The fact that CD33 is not expressed on pluripotent hematopoietic stem cells is a positive advantage as it allows myelosuppression recovery [52].

One mechanism that is postulated to have contributed to the limited clinical efficacy of gemtuzumab ozogamicin is the elevated activity of P-glycoprotein in leukemic blasts, indeed patients responding to gemtuzumab ozogamicin exhibited significantly lower P-glycoprotein activity, namely reduced drug efflux, as compared to patients who did not respond [53]. It is also hypothesized that the acid labile hydrazone linker may have been a contributing factor and hence a liability given its reported short half-life in plasma [54]. In the context of gemtuzumab ozogamicin Mylotarg®, a short half-life is likely to exacerbate toxicity in healthy tissues due to premature release of the active calicheamicin payload as

well as impact potency by compromising efficient internalization of calicheamicin into leukemic blasts [55].

Brentuximab Vedotin (Adcetris®)

The second ADC to receive marketing approval was brentuximab vedotin (Adcetris®), made by conjugation of the potent auristatin tubulin agent (MMAE) to an IgG1 anti-CD30 antibody via a cleavable valine-citrulline (vc) dipeptide linker [56]. The CD30 antigen, a marker for activated lymphocytes, is highly expressed on the Reed–Sternberg cells of Hodgkin lymphoma (HL) as well as on the malignant cells of anaplastic large cell lymphoma (ALCL), indeed it was approved initially for the treatment of relapsed HL and ALCL, then FDA granted an expansion of use to include first-line treatment of stage III and IV HL in combination with chemotherapy (*FDA Press Release. March 2018*) and in 2017 as a treatment for patients with cutaneous T-cell lymphoma (CTCL) who have received prior systemic therapy (*FDA Press Release. November 2017*).

Ado-Trastuzumab Emtansine (Kadcycla®, T-DM1)

The only ADC licensed in non-hematological malignancies is a ado-trastuzumab emtansine (T-DM1, Kadcyla, Roche, Genentech), the antibody used is the well-known trastuzumab (Herceptin®), a humanized IgG1 anti-HER-2 Ab linked with a bifunctional non-cleavable linker, succinimidyl-4-(N-maleimidomethyl)cyclohexane-1-carboxylate (SMCC) stable and attached by random lysines to 3 to 4 maytansoinoids DM1 [34]. The human epidermal growth factor receptor 2 (HER2), known as erbB-2, or proto-oncogene Neu, is a receptor tyrosine-protein kinase, widely studied, encoded by the ERBB2 (HER2) gene on chromosome 17q12 [57]. It is as an oncogenic driver in a subset of breast cancers and the

development of HER2 directed therapies has improved the prognosis of HER2 amplified breast cancers. Ado-trastuzumab emtansine was approved specifically for treatment of HER2-positive metastatic breast cancer (mBC) in patients who have been treated previously with trastuzumab and a taxane (paclitaxel or docetaxel), and who have already been treated for mBC or developed tumor recurrence within six months of adjuvant therapy.

Inotuzumab ozogamicin (Besponsa®)

Inotuzumab ozogamicin is an ADC recently approved in the EU and US for the treatment of adults with relapsed or refractory B-cell precursor acute lymphoblastic leukemia (ALL) r . This conjugate is made up of inotuzumab, a humanized IgG4 anti-CD22 monoclonal antibody linked to an anticancer agent from the calicheamicin class, N-acetyl-γ-calicheamicin via an acid-labile 4-(4-acetylphenoxy)butanoic acid linker [58]. The CD22 receptor is expressed on most B-cell malignancies such as B-cell ALL, chronic lymphocytic leukemia, non-Hodgkin lymphoma (NHL) and hairy cell leukemia, but not in normal tissues, including hematopoietic stem cells and hematopoietic precursors of B lymphocytes. While the function of the transmembrane sialoglycoprotein CD22 is not completely clear, it is thought to regulate B-cell migration, B-lymphocyte survival, signal transduction, B-cell homing and cellular adhesion [59].

2.1.7 CD205 as potential target of solid tumors

CD205 (alias Ly75, DEC-205) is a type I transmembrane protein that belongs to the macrophage mannose receptor family of C-type lectins. The C-type lectin receptors are a large superfamily of multi-functional extracellular proteins containing C-type lectin-like domains (CTLDs), double loop structures with Ca2+-dependent carbohydrate binding activity. The extracellular domain of the protein consists of a cysteine-rich domain (CR), a fibronectin type II domain (FN) and 10 tandemly repeated CTLDs [60-62]. Although structurally related to Mannose Receptor (MR) family, CD205 does not contain the conserved residues required for lectin and C-type lectin binding [63], and the ligands bound by CD205 have remained elusive. The short cytoplasmic tail contains motifs for amino acid-based endocytosis, indeed it is physiologically involved in antigen uptake, processing and presentation by antigen presenting cells and it plays a role in the immune clearance as a recognition receptor for apoptotic and necrotic cells [64].

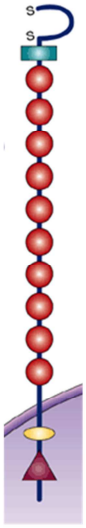

Figure 5. Rapresentation of CD205 receptor. The red dots represent the carbohydrate recognition domains (CRD) or CRD-like domains; the yellow circle represents the tyrosine-based motif for targeting to coated pits and internalization; the red triangle represents the triad of acid aminoacids; the green rectangle represents the fibronectine type II repeat motif.

CD205 is expressed at high levels on cortical thymic epithelium, thymic medullary DCs (CD11c+ CD8+), and subsets of peripheral DCs (CD11c+ CD8+ splenic/lymph node DCs, dermal/interstitial DCs, and Langerhans cells) [65, 66].

Functional studies, using monoclonal antibody anti-CD205 conjugated with an antigen as a surrogate ligand, demonstrates that after the binding, the antigen is endocytosed, processed and presented on both MHC class II and MHC class I molecules with high efficiency and elicit antigen-specific CD4+ and CD8+ T lymphocyte responses. Indeed, depending on the presence or absence of an additional activation signal (i.e. CD40 agonist), it resulted in either immunostimulatory or immunoregulatory effects, respectively [67, 68]. These finding have increased the interest in this antigen in order to design vaccine and improve the targeted immunotherapy.

The endocytic capacity of CD205is abrogated by the presence of small amounts of CD205–DCL1 fusion protein detected in mature DC, indeed Buttler and colleagues suggested that CD205 has two distinct functions – one as an endocytic receptor on immature dendritic cells and a second as a non-endocytic molecule on mature dendritic cells [69]. Furthermore, other researchers found this fusion protein expressed in Hodgkin's lymphoma [70].

In addition to its physiological role in the immune system, it was recently demonstrated thate CD205 influences IL6 signalling and progression of ovarian cancer [71].

Faddoui et al. demonstrated that CD205 is overexpressed in advanced epithelial ovarian cancer (EOC) and its suppression induces mesenchymal-to-epithelial transition (MET) in EOC cell lines with mesenchymal morphology, followed by reduction of their migratory

and invasive capacity in vitro and enhanced tumor cell colonization and metastatic growth in vivo [72].

Using the OGAP® target discovery system and proteomic analysis, we identified CD205 antigen as highly expressed in a range of solid tumors (gastric, pancreatic, bladder, breast and colon) and hematologic lymphomas (multiple myeloma and Diffuse Large B-Cell Lymphoma). Pancreatic cancer, TNBC and Diffuse Large B-Cell Lymphoma (DLBCL) displayed particularly high levels of CD205 [73].

Mass spectrometry of tumor cell membranes demonstrated that CD205 expression is elevated in pancreatic cancer compared to normal pancreas, and in TNBC compared to other breast cancer types. We confirmed and extended these initial proteomic observations by using a specific antibody against CD205 for immunohistochemistry (IHC) evaluation of the protein expression in many different solid tumor types. [73]. Consistent with the proteomics data, strong and specific CD205 staining was detected in TNBC (75% prevalence), bladder cancer (70% prevalence), and pancreatic tumors (68% prevalence), whereas it was much reduced in the corresponding normal tissues using a commercial CD205 antibody.

To further validate the antigen expression in clinical specimens, we evaluated CD205 antigen expression on 103 TNBC, 50 adenopancreatic and 100 urothelial carcinoma samples in collaboration with IRCCS Istituto Nazionale dei Tumori (Milan, Italy). The data showed that CD205 was heterogeneously expressed in the majority of triple negative breast cancer (TNBC) urothelial and in all pancreatic cancer cases, in detail, regardless any intensity staining score, the antigen was expressed in 85% of TNBC, in 100% of pancreatic adenocarcinoma and in 67% of urothelial carcinoma samples [74].

All these CD205 features, such as the rapid and efficient internalization rate, the differential cell surface expression in multiple human cancers compared to healthy tissues together with the high medical need reported in those malignancies, suggest that this antigen might represent a target to be pursued for the development.

2.1.8 MEN1309/OBT076 antibody

MEN1309/OBT076 is a novel anti-CD205 fully humanized IgG1 conjugated through a cleavable N-succinimidyl-4-(2-pyridyldithio) butanoate (SPDB) linker to the microtubule disrupting-agent DM4, that upon the binding with its antigen is delivered to lysosomes by receptor-mediated endocytosis resulting in release of active toxin [73].

It was produced using the human transgenic Xenomouse platform (Amgen, Thousand Oaks, CA). Mice were immunized with CHO cells transfected with full length CD205. Approximately 1400 hybridoma clones were screened for binding specificity to CD205 by flow cytometry on HEK293 cells transfected with full length CD205 and finally MBH1309/OBT076_16A5 was selected as lead clone. A CHO derived cell line was developed using the GS Gene Expression System™ (Lonza, Basel, Switzerland). The variable region sequences for the antibody's heavy and light chain were cloned into the Lonza GS plasmid which was stably expressed in CHO-K1SV cells. MBH1309/OBT076_16A5 was found to bind specifically and with high affinity the CD205 expressed on HPAFII cells (pancreatic adenocarcinoma cell line) with an EC50 of 0.14nM. The antibody is rapidly internalized and re-localized from the cell surface to the cytoplasm of HT-29 cells over a 1 hour time course as measured by IF microscopy.

The MBH1309/OBT076_16A5 human anti-CD205 antibody was initially conjugated to two different antibiotic agents, the maytansinoid DM1 and DM4 toxins through a non-cleavable MMC (4-[N-maleimidomethyl] cyclohexane-1-carboxylate) linker and a cleavable SPDB linkerrespectively (reported as 16A5-MMC-DM1 and 16A5-SPDB-DM4). The antitumor activity of the ADCs was then evaluated in solid and haematological mouse xenograft models. The ADCs showed comparable in vivo antitumor activity against the HPAFII pancreatic cancer xenograft tumor model exhibiting homogeneous expression of the target antigen, whereas, in the Raji DLBCL xenograft tumor model with heterogeneous expression of the CD205 antigen, the in vivo efficacy of 16A5-SPDB-DM4 administrated at 5 mg/Kg was much more potent than that of 16A5-MMC-DM1 administrated at 10 mg/Kg [73]. Based on these data MBH1309/OBT076-SPDB-DM4 (designated MEN1309/OBT076 from here on out) was selected as a lead candidate ADC to target CD205 positive cancers.

The antibody was conjugated to DM4, to produce the MEN1309/OBT076 ADC. The DAR of MEN1309/OBT076 was approximately 1:3.7.

Here we show the in vitro characterization of MEN1309/OBT076 for target binding affinity, mechanism of action, cytotoxic activity against a panel of cancer cell lines and the antitumor activities in different cell-line derived and patient-derived xenograft (PDX) and models. Furthermore, we describe the pharmacokinetics and pharmacodynamics profile of the ADC administrated using different schedules

Our data supported the clinical development of MEN1309/OBT076 in the first-in-human SHUTTLE clinical trial, currently ongoing.

3. Materials and Methods

3.1 Cell lines

All cancer cell lines used were purchased from the American Type Culture Collection - ATCC (Manassas, Virginia, USA) and Deutsche Sammlung von Mikroorganismen und Zellkulturen - DMSZ (Braunschweig, Germany) and cultured following manufacturer instructions. Mycoplasma testing was not performed on in vitro propagated cultures, which were maintained for maximal 4 months. No additional authentication method was performed.

3.2 Antibody internalization

IncuCyte® FabFluor Antibody Labeling Reagents are Fc-region targeting Fab fragments conjugated to a pH-sensitive fluorescent probe. These reagents enable a generic one-step, no-wash, labeling protocol for all isotype matched Fc-containing test antibodies. At pH 7.0, the Fab-Ab complex has little or no fluorescence. When labelled antibodies are added to cells, a fluorogenic signal is observed as the Fab-Ab complex is internalized and processed via acidic (pH 4.5-5.5) lysosomes and endosomes.

Cells were plated (HPAFII, SW780 and HCC-1806) 10K per well on flat-bottom 96 well plates prior to assay.

Test antibody at known concentration (30 nM) was mixed IncuCyte FabFluor reagent at a molar ratio of 1 to 3 in complete growth media.

Following addition of Ab/Fab complex assay plates were immediately placed in an IncuCyte® S3 live-cell analysis system and scanned for HD phase and red fluorescence images at 10x or 20x magnification every 1 hour minutes for up to 48 hours.

Images were automatically analysed using the integrated IncuCyte software for the following metrics phase confluence (measure of cell area), red fluorescence object area (index FabFluor labelled internalized antibody). Top Hat subtraction was used to minimize any background fluorescence signal.

3.3 IHC and visual scoring

The formalin-fixed, paraffin-embedded (FFPE) procedure, was adopted for cell lines, tumor masses derived from xenograft and PDX models. Slides were dewaxed and rehydrated. Antigen retrieval was performed in a Tris pH 9.0 buffer and a standard IHC protocol was used to assess expression of the target antigen. Staining was performed using a mouse monoclonal primary antibody against CD205 (Leica; clone 11A10 [NC-L-DEC205]) and a mouse IgG isotype (R&D Systems; MAB002); concentration matched and used at a dilution of 1:80. The primary antibody was detected with an anti-mouse-HRP labelled secondary antibody polymer (Dako) and positive signal was detected with DAB chromogen. Alternately, the primary antibody was detected with an anti-mouse biotinylated secondary antibody (Dako), followed by incubation with streptavidin peroxidase (Dako) prior to detection with DAB chromogen. Slides were developed, counterstained, and visualized by brightfield microscopy. A scoring system was used to evaluate the CD205 antigen expression according to the observable staining. A score of 3+ denoted strong expression, 2+ indicated moderate expression and 1+ corresponded to weak expression. Samples that did not stain positively for CD205 were scored negative (0).

3.4 Cytotoxicity assay

Tumor cells were incubated with MEN1309/OBT076 for 72 hours at 37°C. Cell viability was measured by alamarBlueTM Cell viability reagent (Thermo Fisher Scientific) according to the manufacturer's instructions. Cells were incubated for 4 hours at 37°C with alamarBlueTM, and fluorescence was measured with an Infinity 200 plate reader (TECAN). Percent viability was calculated using wells incubated in the absence of ADC as the control and was plotted versus antibody concentration. Nonlinear regression, sigmoidal dose-response analysis using GraphPad™ Prism software (GraphPad, La Jolla, CA) was used to calculate EC50 for each assay.

3.5 RNA extraction and quantitative real time PCR detection

Cell lysates and total RNA was prepared with RNeasy Mini Kit (Qiagen) according to manufacturer instructions. The corresponding cDNAs were synthesized using the High-Capacity cDNA Reverse Transcription Kit (Applied Biosystems). To determine the expression levels of the CD205 transcript, duplicates of 1:5 dilutions of cDNA samples were amplified in 25 µl of TaqMan Universal PCR Master Mix using 1.25 µl of the 20X Inventoried Assay purchased from Applied Biosystem. The inventoried assays used were Hs00158966_m1 (Human LY75) and Hs99999905_m1 (human GAPDH as endogenous control), Applied Biosystem. Threshold cycle values (Ct) were selected from the geometric phase of the amplification curves and Ct values greater than 34 were considered not detectable. The amplification and quantitative real time detection was performed in a 7300 Real Time PCR system (Applied Biosystems). Data were presented as mean relative copy number (RCN) using RCN = 2-ΔCt, where ΔCt is the Ct (target) – Ct (GAPDH).

3.6 Estimation of antigen per cells by quantitative flow cytometry

Cell surface CD205 antigen expression levels were measured using BD Bioscience Quantibrite kit. The CD205 antigen density on the selected cancer cell lines was quantified determining the PE-conjugated MEN1309/OBT076 bound per cell. Briefly, special calibrated beads generate a standard curve that converts MFI into fluorochrome molecule number which in turn corresponds to the number of antigens per cell. Adherent cells were detached using 1X Cell Dissociation Non Enzymatic Solution (Sigma Aldrich) and resuspended in PBS + 0.5% BSA (Milteny Biotech). 100 µl of cell solution (3x105 cells) were dispensed in 5 ml flow cytometric tubes and 5 µl of FcR Blocking (Milteny) were added. After ten minutes at 4°C, 10 µl of different dilutions of the PE-conjugated MEN1309/OBT076 (ranging between 0.1 µg/ml to 20 µg/ml) were added. Acquisition of data was carried out using a FACS Canto II. For each sample MFI was determined using FacsDiva software and converted to amount of antigen bound per cell.

3.7 MEN1309/OBT076 binding to FcγRIIIA-158V

An ELISA method was performed to measure the binding affinity of both unconjugated and conjugated MEN1309/OBT076 to FcγRIIIa-158V. Briefly, MaxiSorp 96-well plates (Roskilde, Denmark) were coated with 100 ml/well 2 µg/ml of anti-Tetra His antibody and incubated at 4°C overnight. The plates were washed 4 times with 300 µl/well PBS containing 0.05% Tween 20 and blocked with 100 µl/well PBS containing 0,5% BSA. After 1 hour incubation at room temperature and washing 100 µl/well of 1.5 µg/ml FcγRIIIa-158V (Sino Biologicals) were added to plates and incubated at room temperature for 1

hour. After washing, 100 µl/well of three-fold serial dilutions of antibodies were incubated at room temperature for 2 hours. Bound antibodies were detected using (1:40000) peroxidase-labelled goat antihuman IgG F (ab') 2 fragment specific (Jackson ImmunoResearch Laboratories) and 100 µl/well 3,3',5,5'-Tetramethylbenzidine (TMB) as substrate (Thermo scientific, Waltham, MA, USA). The reaction was stopped with 100 µl/well Stop solution, and the absorbance at 450 nm was measured on an Infinite M200 plate reader (Tecan, Switzerland).

3.8 ADCC assay

The ADCC assay was performed using the ADCC Reporter Bioassay from Promega, following the kit instructions with some modifications. Briefly, 4x106 THP-1 target cells were washed and re-suspended in 4 mL of ADCC buffer and were seeded on a white 96-well plate. Serial dilutions of antibodies, ranging from 0.3 ng/mL up to 1 µg/mL, were seeded adding a further volume of 25 µl/well. Jurkat effector cells were prepared by adding to 630 µl cells from the stock vial to 3600 µl of ADCC buffer. 25 ul of this dilution were added to each well obtaining a Effector / Target cell Ratio = 3 / 1 (75000 / 25000). Plates were incubated 6h at 37°C. After a second incubation at RT for 15 min, 75 ul of BioGlo reagent/well were added. Plates were maintained 1 min in the dark and then the developed luminescence was detected in the Infinite M200 reader.

3.9 CDC assay

The CDC assay was performed using purified human serum complement (Quidel, San Diego, CA). MEN1309 (100 µg/ml-0,00001 µg/ml) was diluted with RHB buffer (RPMI 1640 No Phenol Red, Life Technologies, 20 mM HEPES, pH 7.2, 2 mM glutamine, 0.1% BSA). Raji cells were washed in RHB buffer and resuspended at a density of $1x10^6$ cells/ml. In a typical assay, 50 µl of a cell suspension (50,000 cells/well), 50 µl of diluted human complement (4%) and 50 µl of diluted MEN1309 were added to a flat-bottom tissue culture 96-well plate. A control curve with Rituximab antibody was added. The mixture was incubated for 3 hours at 37°C in a 5% CO2 incubator to facilitate complement-mediated cell lysis. Then, 50 µl of Alamar Blue (Accumed International, Westlake, OH) was added to each well and incubated overnight at 37°C. Fluorescence was read using a 96-well fluorometer with excitation at 530 nm and emission at 590 nm. The results are expressed in relative percentage of cytotoxicity that is proportional to the number of viable cells. The percent CDC activity was calculated as follows: 100 - [(RFU test/RFU background) x100].

3.10 In vivo studies

The human tumor xenograft studies were performed at Menarini Ricerche facility, Charles River Discovery Research (Morrisville, NC) or Washington Biotechnology (Simpsonville, MD). The athymic female nude mice (outbred, CD-1/nude) or female FOX Chase SCID (CB17/Icr-Prkdcscid/IcrIcoCrl) 5-8 weeks old, were purchased from Charles River, maintained in microisolator cages under continuously monitored environmental conditions. Drinking water and specific sterilized diet (VRF1, Charles River) were supplied

ad libitum. Environmental conditions, as well as the procedures for housing and handling the animals, were in compliance with the UKCCR guidelines [75] and the European Convention for the protection of vertebrate animals used for experimental and other scientific purposes [Directive 2010/63/Eu Of The European Parliament And Of The Council On The Protection Of Animals Used For Scientific Purposes] or the Association for Assessment and Accreditation of Laboratory Animal Care International.

5×10^6 - 2×10^7 cells with or without matrigel, were injected subcutaneously into the flanks of mice. Tumor growth was followed by caliper measurement of length and width several times weekly. Tumor volume (expressed as mm3) was calculated using the following formula [76]: length (mm) x width^2 (mm)/2.

The body weight of mice was also monitored. The treatments were started when average tumor volume reached 88-300 mm3. Animals were randomly assigned into groups (6 mice/group), and treated with MEN1309/OBT076 intravenously (i.v.) either with a single dose, once weekly for 2 consecutive weeks (q7dx2), or every 3 weeks for 3 consecutive weeks (q21dx3). The dose of MEN1309/OBT076 administered to mice ranged from 1.25 mg/kg to 10 mg/kg. Tumor Volume Inhibition % (TVI%) in treated versus control mice was determined after the last drug treatment and at the nadir of tumor volume. Mice were euthanized when tumors reached 2000 mm3 or when the study endpoint was reached.

The murine response criteria (mRECIST) used follows the modified Response Evaluation Criteria in Solid Tumors (RECIST). The mRECIST criteria were applied only to mice [77] that completed the efficacy study, while mice sacrificed earlier (for either ethical or pharmacodynamics reasons) were not included.

3.11 In vivo studies on PDX models

The antitumor activities of MEN1309 on patient-derived xenograft (PDX) models were carried out at the Lab Animal Service (LAS) at Campus Vall d'Hebron Animal Facility by the Growth Factors laboratory of Vall D'Hebron Institute of Oncology (VHIO), Barcelona, Spain and at Champions Oncology, Inc., Baltimora, USA.

3.12 Mouse pharmacokinetics design

The tumor bearing and non-tumor bearing mice were treated with a single i.v. administration of MEN1309/OBT076 at 5 mg/kg and sacrificed after 5, 30 minutes, 1, 3, 24, 48, 72, 96, 144, 192, 240, 288, 384, 504, 672 and 816 hours, at which times samples (whole blood, tumor mass and liver) were harvested. Three mice were used for each time point. To obtain the serum sample from the whole blood, the samples were left on the bench for 30 minutes at room temperature, to complete the coagulation process and then they were centrifuged at 3000 RPM for 10 minutes at room temperature. We collected 250 µl of serum from each blood sample and stored it at -80°C.

3.13 MEN1309/OBT076 serum determination in mice

An indirect ELISA system was used. The plate coating was performed using 100 µL/well of 2 µg/mL of CD205 antigen (OBT076ECD) solution. The plate was covered and stored at +4°C for at least 12 hours and at the most for 3 days. After coating, the blocking was as follow: the plate was washed for three times with 300 µL/well of PBS 1X 0.05% Tween-20, then each well was filled with 200 µL of PBS 1X, 0.05% Tween-20 – 2% BSA. The plate was

covered and incubated under stirring (350 rpm) for two hours at room temperature. MEN1309 linkage (detected antibody), following the blocking, the plate was washed for three times with 300 µL/well of PBS 1X 0.05% Tween-20, then 100 µL of each sample were plated in duplicate, following the daily scheme. The plate was covered and incubated under stirring (350 rpm) for one hour at 37°C. Secondary antibody linkage (enzyme labeled), following the MEN1309 linkage, the plate was washed for three times with 300 µL/well of PBS 1X, 0.05% Tween-20, then each well was filled with 50 µL of Biotin Anti maytansine antibody 50 ng/mL in buffer. The plate was covered and incubated under stirring (350 rpm) for one hour at 37°C. Streptavidin poly-HRP40 conjugated linkage: following the Biotin anti maytansinoid antibody linkage, the plate was washed for three times with 300 µl/well of PBS 1X, 0.05% Tween-20, then each well was filled with 100 µL of Strepatvidin poly-HRP40 conjugated diluted 1:10000 in buffer. The plate was covered and incubated under stirring (350 rpm) for one hour at 37°C. Following the enzyme labeled, for colour development (enzymatic reaction), the plate was washed for three times with 300 µL/well of PBS 1X, 0.05% Tween-20, and then 100 µL of the substrate/chromophore TMB was added. The plate was covered and incubated without stirring at 37°C for 10 minutes. The enzymatic reaction was stopped by adding 100 µL/well of the 1 N HCl, and then the plate was immediately read.

3.14 Phospho-histone H3 Immunofluorescence

To visualize the histone H3 (phospho S10) protein, formalin-fixed, paraffin-embedded tumor mass sections were deparaffinized and hydrated. Unmasking of antigenic sites was performed in Target Retrieval Solution pH 9.00 for 6 minutes in a microwave oven at

100°C and 650 W. Sections were incubated in permeabilization buffer (PBS + 1% BSA, + 0.3% Triton x-100) for 30 min. at room temperature, then blocked in PBS + 5% normal goat serum + 1% BSA for 1h at room temperature. Sections were then incubated with rabbit polyclonal (Abcam ab47297) anti-histone H3 (phospho S10) diluted 1:1000 in blocking buffer overnight at 4°C. After 3 x 5 minutes washes with PBS, the slides were incubated with goat anti-rabbit secondary antibody, Alexa 594 (R37117) for 1h at room temperature. After 3 x 5 minutes washes with PBS, the slides were mounted in Vectashield (H-1200 Vector Laboratories) with DAPI (4', 6-diamidin-2-fenilindolo). The stained sections were visualized with a Leitz Diaplan fluorescent microscope and the images were captured with a Leica DFC450 C camera at 25X. The images were exported from the Leica software and analysed using ImageJ software. Each image was converted to "binary" colour. Nonspecific signals and background were removed using the program function "Despeckly". The "Withwater" function was used to divide the adjacent nuclei. The "analyse particles" function was used to count the total nuclei in the image and "250-infinity" was used to limit the size. The positive cells were counted manually with the function "cell counter".

3.15 Statistical Analyses

GraphPad Prism software (GraphPad Software Inc., California) was used for statistical analysis. Statistical differences were considered to be significant at p-value < 0.05 using the two-tailed Mann-Whitney rank test. In vivo data are presented as mean, with the value for each group represented as a symbol of different shape and line of different colour.

4. Results

4.1 Evaluation of CD205 expression in a panel of human cancer cell lines

The expression of the CD205 antigen was evaluated in a panel of human pancreatic, bladder, colon cancer and TNBC cell lines. The expression level of CD205 mRNA was evaluated by real time quantitative PCR (RT-qPCR) and the results were expressed as Relative Copy Number (RCN), whereas the expression of the protein was characterized by IHC staining and the surface localization of the protein was determined by fluorescent-activated cell sorting (FACS).

The expression of the CD205 antigen in the analysed cancer cell lines was quite heterogeneous; within each histotype the antigen expression ranged from strongly positive to completely negative. The expression data results were very consistent among the three different techniques and in all cases the highest expression level of the CD205 antigen was observed in several pancreatic and TNBC cell lines (Table 1).

Cell line	Tissue	RT-qPCR (RCN)	FACS (No. Antigen per cell)	IHC Score (Cell block)
HPAFII	pancreas	0.95	44576	+++
THP-1	pheripheral blood	0.66	17205	++
HT29	colon	0.53	49765	+++
HCC-1806	breast (TNBC)	0.38	7337	+
BxPC3	Pancreas	0.35	-	+++/++
HCC-70	breast (TNBC)	0.26	-	++/+
SW780	urinary bladder	0.23	8000	++
SU.86.86	Pancreas	0.22	26781	++/+
5637	urinary bladder	0.17	-	-
HCC-1143	breast (TNBC)	0.12	-	++/+
MDA-MB-468	breast (TNBC)	0.12	-	+++
MDA-MB-231	breast (TNBC)	0.057	-	-
TOLEDO	pheripheral blood	0.05	798	-
HT1376	urinary bladder	0.05	-	0
ScaBER	urinary bladder	0.04	-	0
AspC1	pancreas	< 0.01	1305	0
BT-20	breast (TNBC)	< 0.01	-	-
TCC-SUP	urinary bladder	< 0.01	-	-
HT1197	urinary bladder	< 0.01	-	0
MCF-7	breast	< 0.01	-	0
UMUC3	urinary bladder	< 0.01	-	0

- = not tested

Table 1. CD205 expression in human cancer cell lines. The expression of CD205 was characterized in a panel of human cancer cell lines of different histotypes. IHC staining score: - = not tested; 0 = no staining; + = weak staining; ++ = moderate staining; +++ = strong staining.

4.2 CD205 internalization

Using the Incucyte® technology, we assessed internalization rate and localization of unconjugated MEN1309/OBT076 upon its binding to CD205 antigen in tumor cells expressing different levels of the antigen (IHC score: HPAFII 3+, SW780 2+, HCC-1806 1+). The amount of fluorescent monoclonal antibody, delivered inside the tumor cells by lysosomes, increased in a time depend manner and the quantification of the associated

fluorescence signal correlated with the levels of the antigen expressed by the different tumor cells analyzed (Figure 6-7).

These data indicate that CD205 undergoes efficient internalization following engagement by the MEN1309/OBT076 unconjugated antibody.

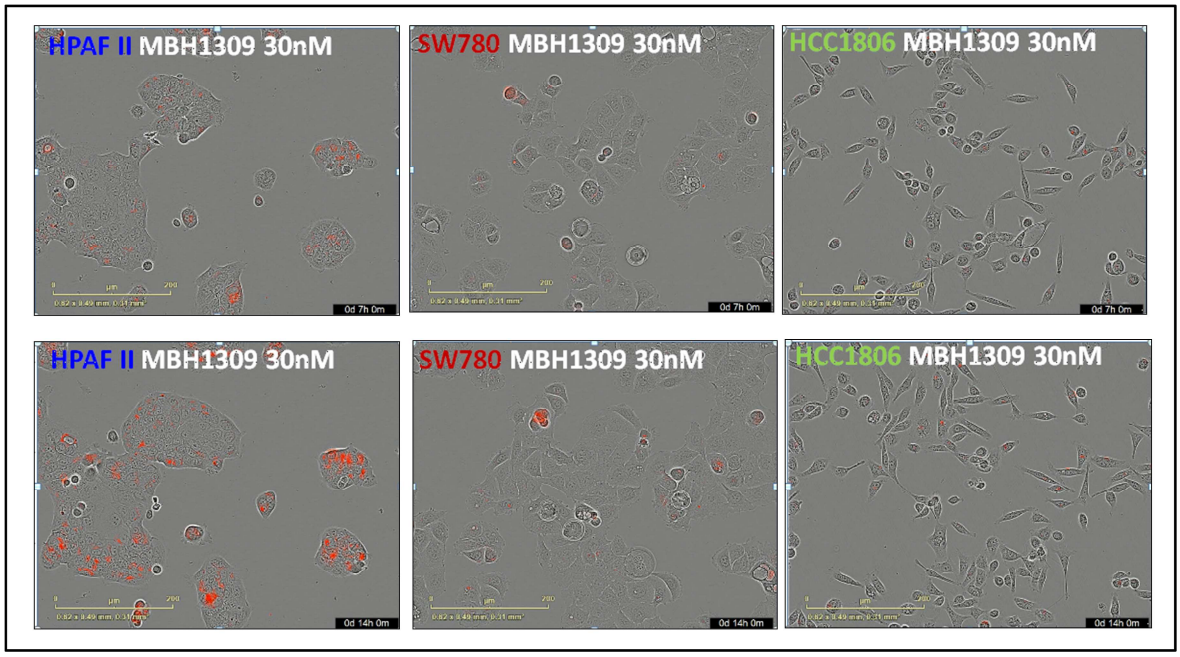

Figure 6. MEN1309/OBT076 unconjugated internalization. Representative images of unconjugated MEN1309/OBT076 internalization in different cancer cell lines after 7h and 14h (upper and lower panel respectively).

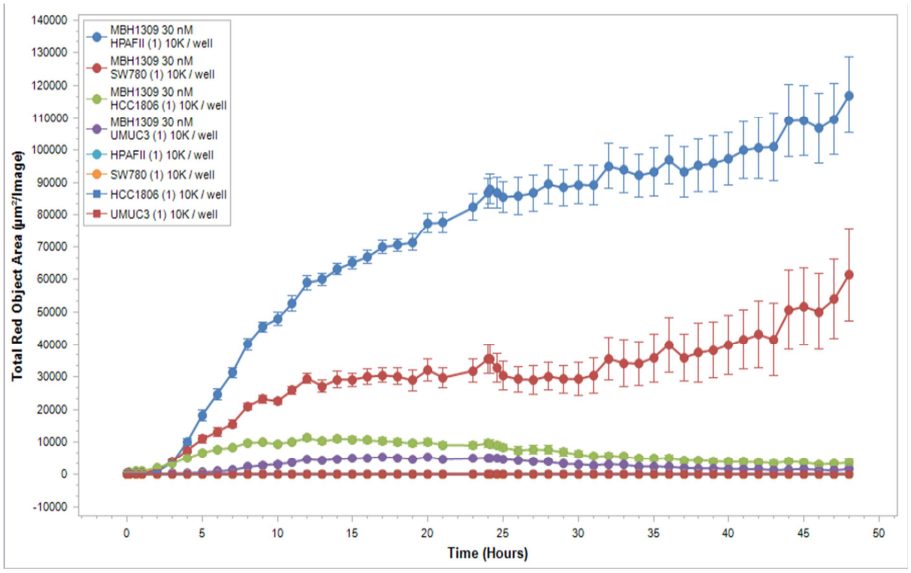

Figure 7. Quantification of internalization. Fluorescence signal quantification of internalized unconjugated MEN1309/OBT076 over time.

4.3 MEN1309/OBT076 cytotoxic activity

Pancreatic, bladder, and TNBC cell lines were used as in vitro models to assess the cytotoxic activity of MEN1309/OBT076. The ADC showed a potent cytotoxic effect on antigen positive cells, with EC_{50} values in the order of nanomolar range (Figure 8). Moreover, the anti-proliferative impact of the ADC was demonstrated against cell lines expressing high as well as low to moderate levels of the antigen. On the contrary, MEN1309/OBT076 showed a negligible effect on CD205 negative cells.

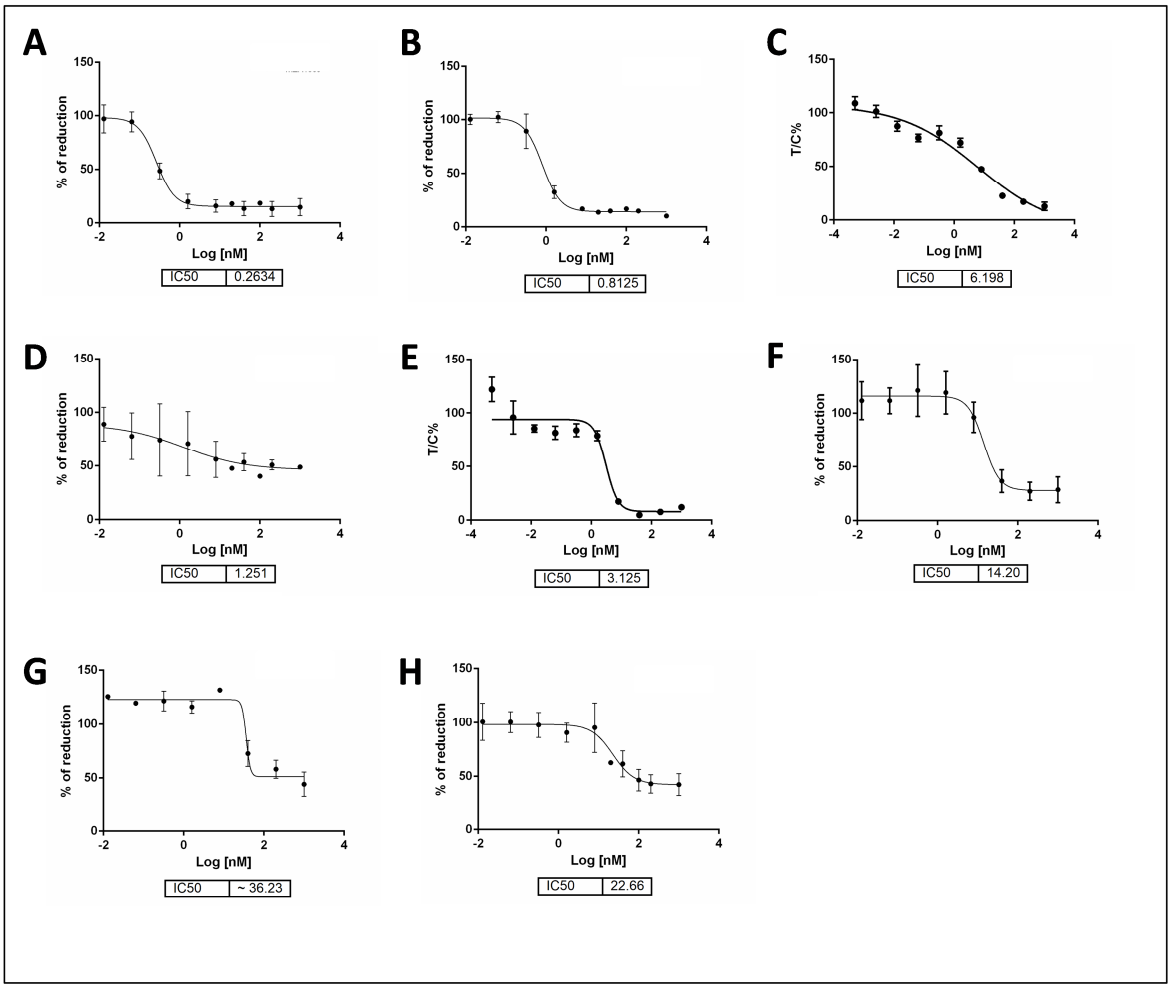

Figure 8. Cytotoxic activity of MEN1309/OBT076 on human cancer cell lines. A, Bladder cancer cell lines SW780; B, TNBC cancer cell line HCC1806; C, TNBC cancer cell line HCC70; D, pancreatic cancer cell line HPAFII; E, bladder cancer cell line 5637; F, breast cancer cell line MCF7; G, bladder cancer cell line HT1197; H, pancreatic cancer cell line AsPc1.

4.4 MEN1309/OBT076 binds to FcγRIIA without inducing any ADCC or CDC response

We then assessed MEN1309/OBT076 for its binding affinity to the CD205 antigen on the THP1 cell line as well as its affinity to the FcγRIIIA receptor and propensity for participating in putative alternative mechanisms of action such as antibody dependent cellular cytotoxicity (ADCC) and complement dependent cytotoxicity (CDC).

FACS binding experiment on THP-1 cell line, performed by titrating unlabeled antibody with a constant amount of labelled antibody, showed high binding affinity of MBH1309/OBT076 to CD205 expressed on the cell surface with no affinity loss after conjugation to DM4 (Figure 9A).

In the ADCC bioluminescence assay, we used THP-1 as target cells, , because they express both CD205 and the antigen recognized by our internal ADCC mAB as positive control. Data showed that, despite its ability to bind FcγRIIIA (Figure 9B), MBH1309/OBT076 didn't induce any ADCC response (the same result was obtained with the control isotype), whereas our internal positive control mounted an ADCC response (Figure 9C).

In vitro CDC assay on Raji cancer cell lines, expressing both CD205 and CD20 antigens, showed no CDC activity when incubated with purified human complement. On the contrary, our positive control Rituximab, showed a strong induction of CDC activity

(Figure 9D). These data suggest that the therapeutic effect of MEN1309/OBT076 is relying primarily on an ADC based mechanism of action.

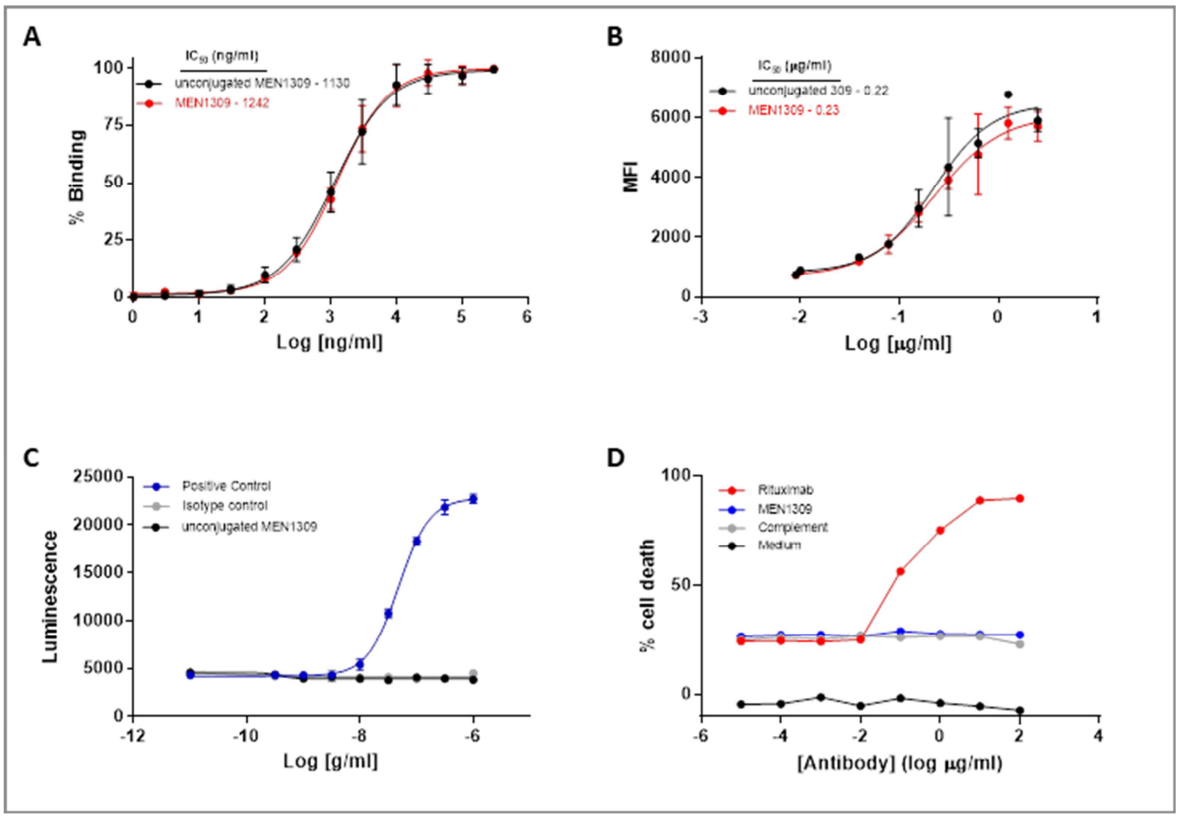

Figure 9: In vitro evaluation of MEN1309/OBT076 additional potential mechanisms of action. A) ELISA assay showed that both unconjugated and DM4-conjugated antibodies were able to bind FcγRIIIA with the same affinity (n=2). B) FACS binding experiment on THP-1 cell line, performed by titrating unlabeled antibody with a constant amount of labelled antibody, showed high binding affinity of MBH1309/OBT076 to CD205 expressed on the cell surface with no affinity loss after conjugation (N=2). C) In vitro ADCC bioluminescence assay showed that, despite the ability to bind FcγRIIIA, MBH1309/OBT076 didn't induce any ADCC response. D) In vitro CDC assay on Raji cancer cell lines showed no CDC activity of MBH1309/OBT076 when incubated with purified human complement. On the contrary, Rituximab (used as positive control), showed a strong induction of CDC activity.

4.5 MEN1309/OBT076 in vivo efficacy in CD205 expressing xenografts and PDX models

To test the in vivo efficacy of MEN1309/OBT076, different cell-based and patient-derived xenograft models were selected on the basis of the IHC analysis for CD205 staining in various tumor types (Table 2).

Xenografts	Membrane Score[b]	Heterogeneous Expression
HPAFII	3+	HO
AsPc-1	0	nd
HCC-1806	1+	HO
HCC-70	1+	HO
SW780	2+	HO
PC-PDX6Pa	3+	HO
PDX21[a]	1+	HO
PDX347[a]	3+	HO
PDX22[a]	1+	HO
CTG-1388[a]	2+	HE
CTG-1652[a]	2+	HE

Table 2. Characterization of CD205 expression by IHC in a panel of human cell lines and patient derived xenografts. [a)] PDX models. [b)] Membrane score represents the staining intensity. HE = heterogeneous. HO = homogeneous.

Efficacy of MEN1309/OBT076, administered with a q21dx3 schedule, was determined by assessing the inhibition of tumor growth at the nadir of tumor volume in treated vs.

control mice and applying the mRECIST criteria adapted to the mouse from human RECIST (78). No toxic effects of MEN1309/OBT076 were observed in any of the studies.

Triple Negative Breast Cancer (TNBC). In two xenograft models of TNBC, HCC-1806 and HCC-70, classified as low antigen expressing cell lines by IHC quantification (score of 1+), MEN1309/OBT076 showed an impressive antitumor activity (Figure 10A-D). In both models, 5mg/kg MEN1309 resulted in complete tumor regression in all the treated animals (5/5), with a TVI of 99% for both models, evaluated one week after the last treatment (Figure 10B-C-E-F). The MEN1309/OBT076-mediated reduction in tumor growth was dose-dependent. MEN1309/OBT076 at 3.5 mg/Kg induced a TVI of 93% and 91% in HCC-1806 and HCC-70 xenograft models respectively (Figure 5B-C-E-F). Based on mRECIST criteria analysis, in HCC-1806 xenografts we observed a complete response in 3 out of 5 mice (60%), one partial response (1/5) and one stable disease; while in HCC-70 xenografts we observed a complete response in 4 out of 5 mice (80%) and one stable disease (1/5) (Figure 10B-C-E-F). Antitumor activity was also observed at 2.5 mg/kg, with a complete response in 60% of the mice carrying HCC-1806 tumors (3/5) with a TVI of 87% and in 80% of treated mice carrying HCC-70 tumors (4/5) with 98% of TVI, according to mRECIST criteria (Figure 4A-B). Unexpectedly, the administration of IgG1-DM4 control ADC showed a very slight effect on tumor growth (Figure 10 B-C-E-F).

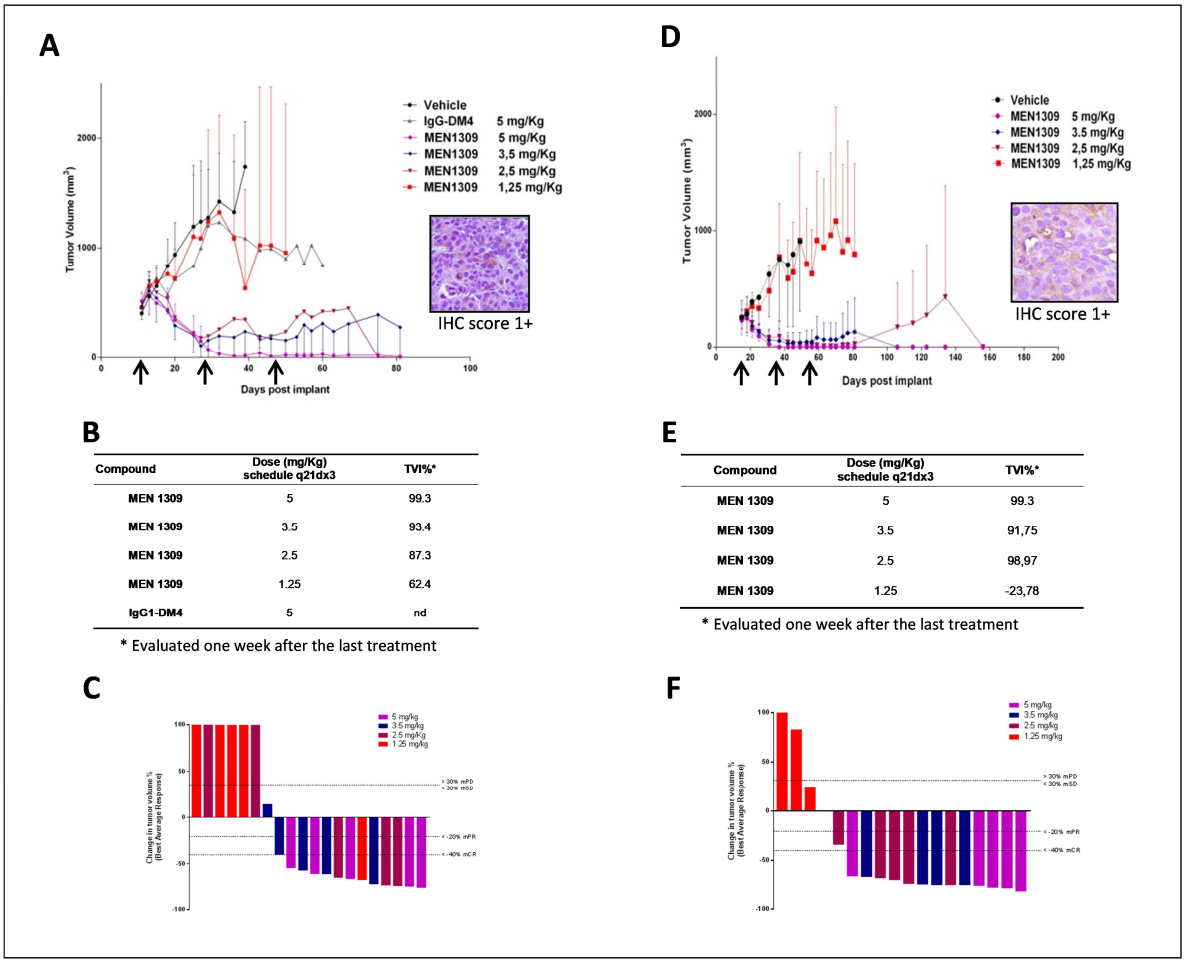

Compound	Dose (mg/Kg) schedule q21dx3	TVI%*
MEN 1309	5	99.3
MEN 1309	3.5	93.4
MEN 1309	2.5	87.3
MEN 1309	1.25	62.4
IgG1-DM4	5	nd

* Evaluated one week after the last treatment

Compound	Dose (mg/Kg) schedule q21dx3	TVI%*
MEN 1309	5	99.3
MEN 1309	3.5	91,75
MEN 1309	2.5	98,97
MEN 1309	1.25	-23,78

* Evaluated one week after the last treatment

Figure 10. MEN1309/OBT076 antitumor efficacy against human TNBC. HCC-1806 (A) and HCC-70 (D) tumor cell lines. A-D: For each tumor model IHC staining, CD205 score, and tumor growth curves are reported; B-E: Tumor Volume Inhibition (TVI%) and C-F: waterfall plots. According to mRECIST criteria response was evaluated one week after the last treatment. Each bar represents a single mouse: mCR Complete Response; mPR, Partial Response; mSD, Stable Disease; mPD, Progressive Disease.

IHC for CD205 expression evaluated on the residual tumor masses 16 days after the first treatment showed that, in the HCC-1806 xenograft model, all doses of the administered drug cleared antigen-positive tumor cells, whereas in the HCC-70 xenograft model, low antigen expression persisted in the tumor cells from all the treated groups (Figure 11).

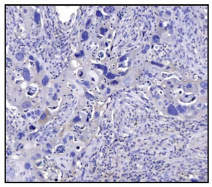

Figure 11. CD205 expression on residual treated tumor mass. Representative image of IHC staining for CD205 in a tumor mass from HCC-70 xenograft model, 16 days after the initial treatment with 5 mg/kg of MEN1309/OBT076. The semiquantitative IHC analysis showed a score of 1+ in 30% of the cells while the remaining were scored as negative (0).

Furthermore, the antitumor activity of MEN1309/OBT076 was also evaluated in PDX models of triple negative breast cancer. As shown in Figure 8A, MEN1309/OBT076 demonstrated significant antitumor activity against PDX-347, characterized by strong (score of 3+) and homogenous CD205 tumor staining. Importantly, at the study endpoint, four out of six mice (66%) treated at 5 mg/kg had a complete and long lasting response (mCR) according to mRECIST criteria and showed a 99.5% of TVI (Figure 12B-C). IHC on tumor tissue samples after two cycles of treatment revealed that the tumors were mainly composed of fibrotic tissue and few cells with a moderate expression of the target antigen (Figure 13). Positive, though less robust results, were also observed on PDX-22, characterized by a low level (score of 1+) of positivity to CD205 (Figure 12 D), showing a TVI of 47.3% without objective response, according to mRECIST criteria (Figure 12E-F).

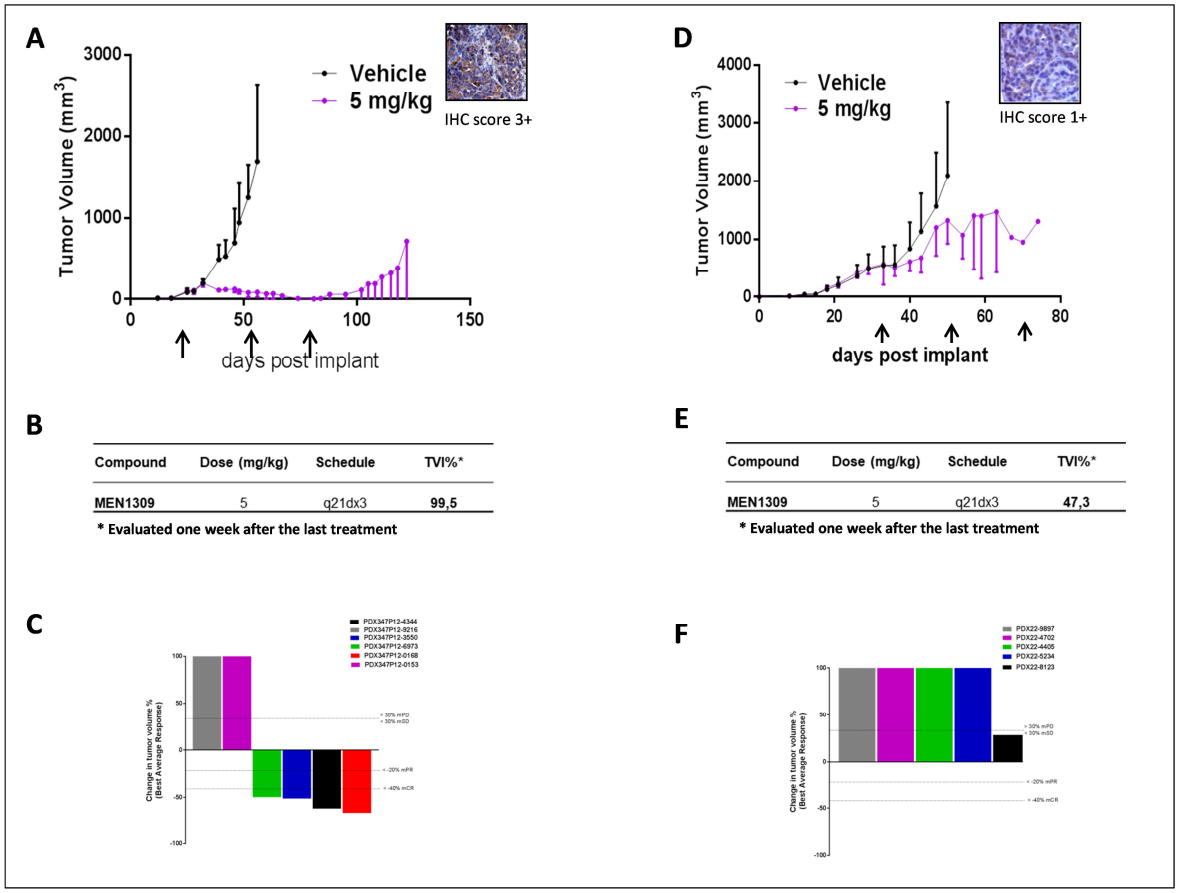

Figure 12. MEN1309/OBT076 antitumor efficacy against human TNBC PDX model. PDX-347 (A) and PDX-22 (D). A-D: For each tumor model, IHC staining, CD205 score and, tumor growth curves are reported; B-E: Tumor Volume Inhibition (TVI%) and C-F: waterfall plots. According to mRECIST criteria, response was evaluated one week after the last treatment. Each bar represents a single mouse: mCR Complete Response; mPR, Partial Response; mSD, Stable Disease; mPD, Progressive Disease.

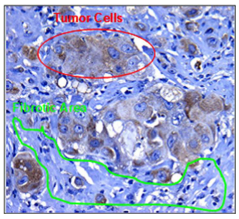

Figure 13. CD205 expression on treated residual tumor mass. Representative image of IHC staining for CD205 in a tumor mass from PDX-347 model, 16 days far from the initial treatment with 5 mg/kg of MEN1309/OBT076. The semiquantitative IHC analysis showed a score of 2+ in 100% of cells. Red and green lines represent, respectively tumor and fibrotic areas.

Pancreatic cancer. In HPAFII, a xenograft model of pancreatic adenocarcinoma in which tumors exhibited strong CD205 expression (score of 3+), potent MEN1309/OBT076-mediated antitumor activity was observed in mice treated with 5 mg/kg of the drug (Figure 14A). Complete regression was observed in 50% of the treated mice, togheter with a TVI of 98.8%. Two additional schedules of 2.5 mg/Kg and 1.25 mg/Kg, showed a TVI of 30.8% and 23.9% respectively, but no objective response was ever observed. IgG1-DM4 produced a very slight effect on tumor growth (Figure 14B-C). On the contrary, no activity was observed in the AsPC-1 pancreatic adenocarcinoma xenograft model (characterized by lack of CD205 antigen expression), at anyof the tested dose (Figure 14D-E-F).

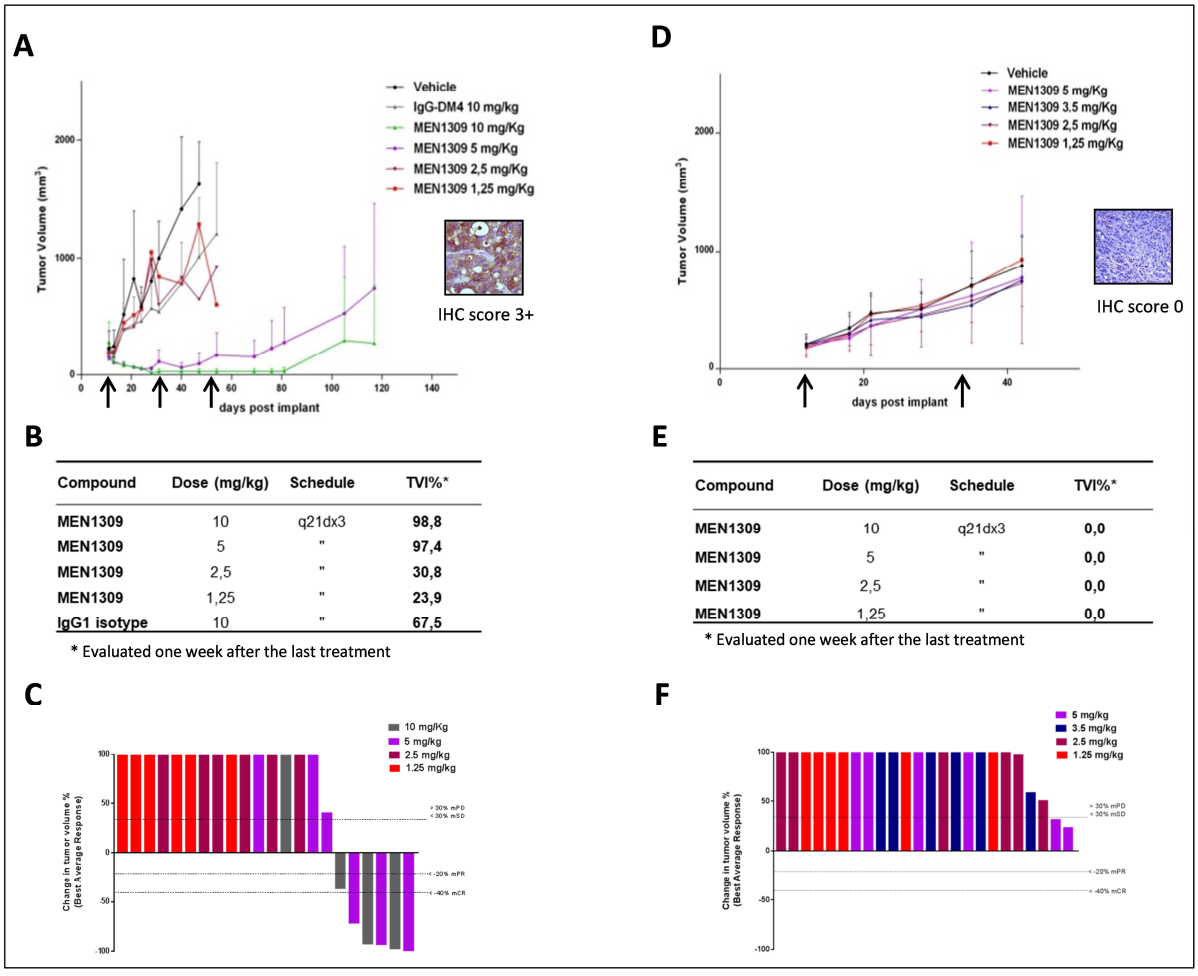

Figure 14. MEN1309/OBT076 antitumor efficacy against human pancreatic adenocarcinoma xenograft models. HPAFII (A) and AsPC1 (D) tumor cell lines. A-D: For each tumor model, IHC staining, CD205 score, and tumor growth curves are reported; B-E: Tumor Volume Inhibition (TVI%) and C-F: waterfall plots. According to mRECIST criteria, response was

evaluated one week after the last treatment. Each bar represents a single mouse: mCR Complete Response; mPR, Partial Response; mSD, Stable Disease; mPD, Progressive Disease.

In PDX-21, a pancreatic cancer model with a weak and heterogeneous CD205 expression, treatment with 5 mg/kg resulted in a complete response in 1 out of 6 mice and a partial response in 1 out of 6 mice according to the mRECIST criteria (Figure 15A-B-C) and a TVI of 49.1%. This efficacy data, although encouraging, are modest when compared to the results observed in PDXs expressing high levels of CD205. To this respect, in the P6P model, characterized by high and homogeneous CD205 expression, we observed 73.7% of TVI (Figure 15D-E-F).

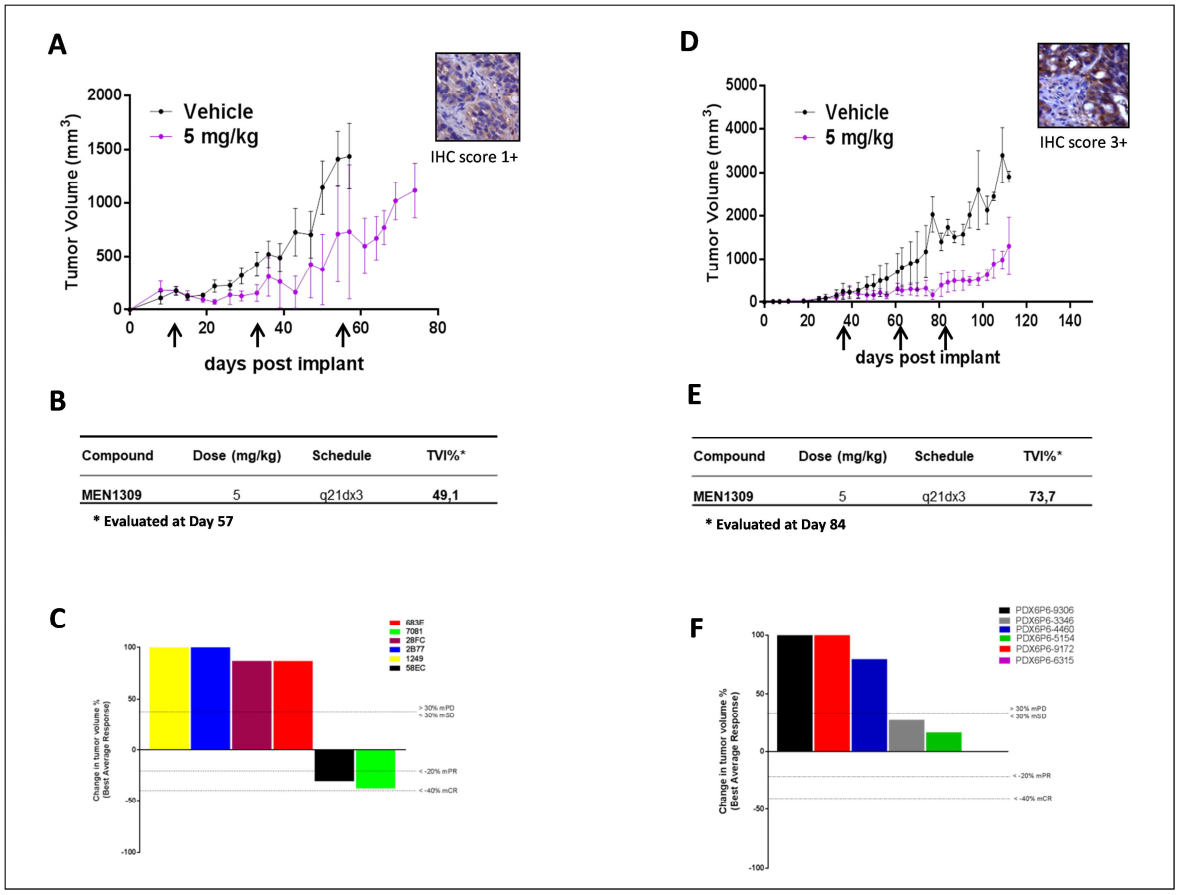

Figure 15. MEN1309/OBT076 antitumor efficacy against human pancreatic adenocarcinoma PDX models. PDX-21 (A) and PDX-P6P (D). A-D: For each tumor model, IHC staining, CD205 score, and tumor growth curves are reported. B-E: Tumor Volume Inhibition (TVI%) and C-F: waterfall plots. According to mRECIST criteria, response was evaluated one week after the last treatment. Each bar represents a single mouse: mCR Complete Response; mPR, Partial Response; mSD, Stable Disease; mPD, Progressive Disease.

Bladder cancer. In the human bladder carcinoma SW780 xenograft model (score of 2+), MEN1309/OBT076 was able to induce a complete response in all mice treated with 10 or 5 mg/kg, and to achieve a TVI of 100%. The 2.5 mg/kg schedule, was also quite effective, with complete response in 2 out of 5 animals and TVI of 94.7%. On the contrary, the 1.25 mg/Kg schedule induced only stable or progressive disease (Figure 16A-B-C). In contrast, either the free cytotoxic payload DM4 or the control isotype administered at an equimolar concentration (200µg/kg) didn't show any antitumor activity.

A

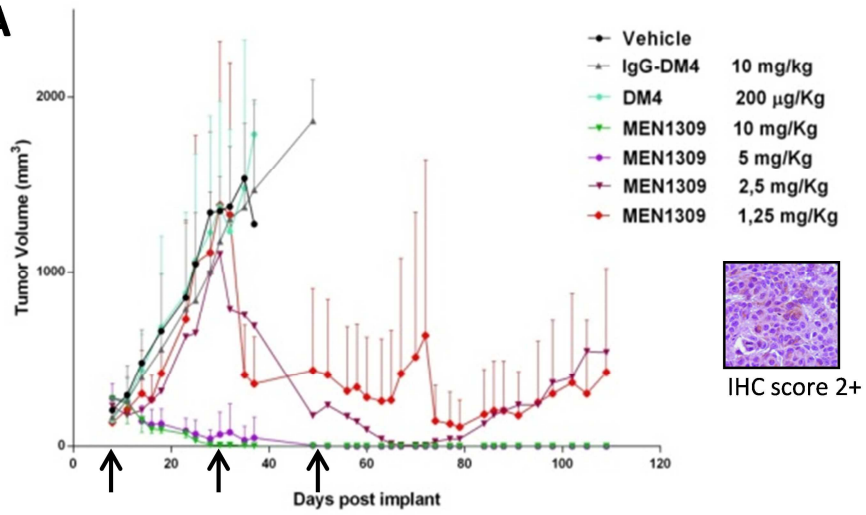

IHC score 2+

B

Compound	Dose (mg/Kg) schedule q21dx3	TVI%*
MEN 1309	10	100
MEN 1309	5	100
MEN 1309	2.5	94.7
MEN 1309	1.25	84.3
IgG1-DM4	10	nd
DM4	0.2	nd

* Evaluated one week after the last treatment

C

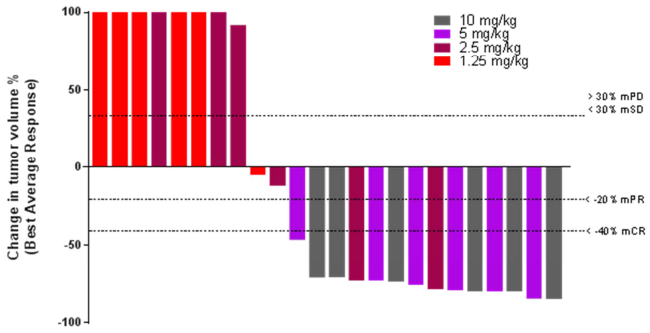

Figure 16. MEN1309/OBT076 antitumor efficacy in SW780 human bladder xenograft model. A: IHC staining, CD205 score, and tumor growth curve is reported B: Tumor Volume Inhibition (TVI%) and C: waterfall plot. According to mRECIST criteria, response was evaluated one week after the last treatment. Each bar represents a single mouse: mCR Complete Response; mPR, Partial Response; mSD, Stable Disease; mPD, Progressive Disease.

Modest findings were observed in PDX models (Figure 17A-D). In both models tested (score of 2+), the mRECIST evaluation indicated one complete and one partial response only (Figure 17B-C-E-F).

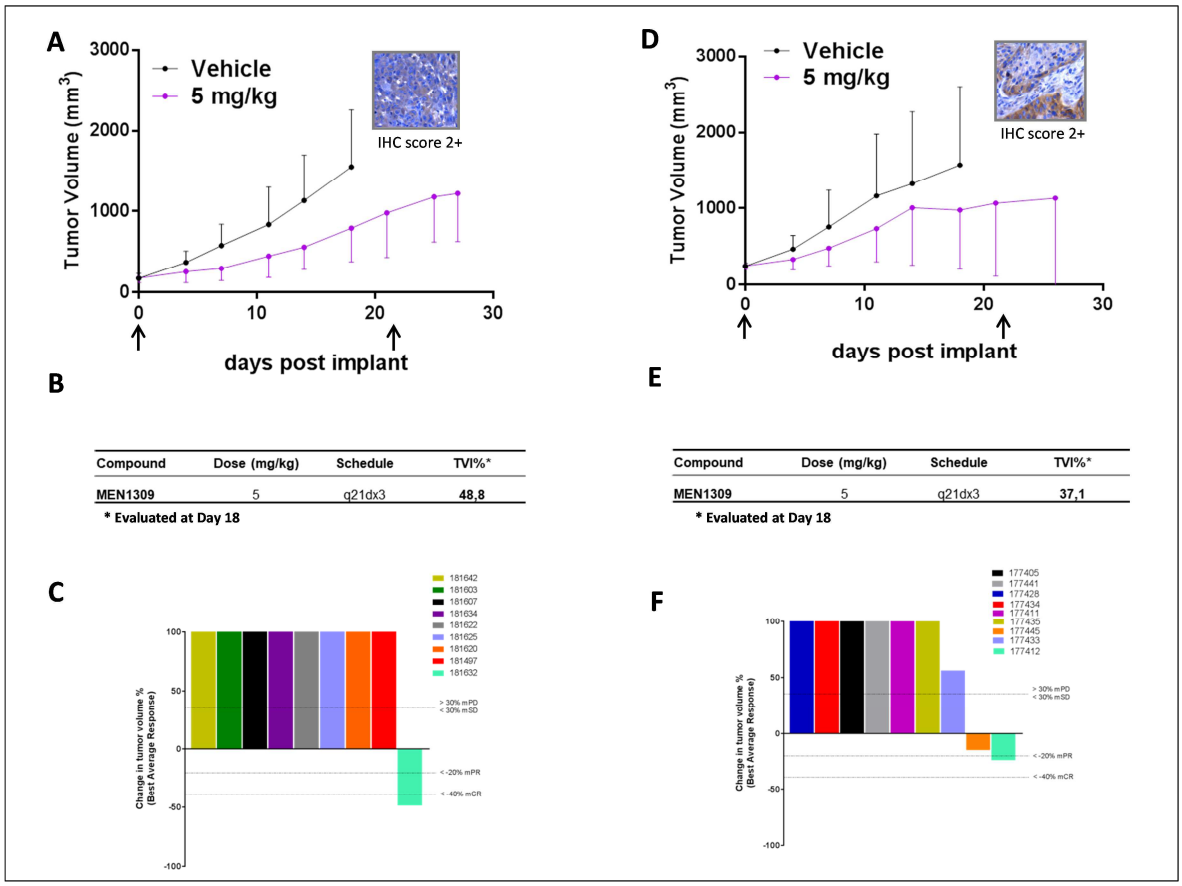

Figure 17. MEN1309/OBT076 antitumor efficacy against human bladder carcinoma PDX models. PDX-CTG-1388 (A) and PDX-CTG-1652 (D). A-D: For each tumor model. IHC staining, CD205 score, and tumor growth curves are reported. B-E: Tumor Volume Inhibition (TVI%) and C-F: waterfall plots. According to mRECIST criteria, response was evaluated one week after the last treatment. Each bar represents a single mouse: mCR Complete Response; mPR, Partial Response; mSD, Stable Disease; mPD, Progressive Disease.

4.6 Pharmacokinetics, pharmacodynamics and toxicity profile of MEN1309/OBT076

The PK profile of MEN1309/OBT076 was analysed after single i.v. administration at 5 mg/Kg in HPAFII pancreatic xenograft bearing mice (characterized by a strong CD205 expression and 3+ IHC score), when average tumor volume reached 200 mm^3, and in non-tumor bearing mice. The associated pharmacodynamics (PD) of the ADC was also analyzed. Due to the molecular mechanism of DM4, the phosphorylation of histone H3 on Serine10, was used as a biomarker of mitotic arrest in the tumor mass [78]. The PK profile of MEN1309/OBT076 was comparable in tumor-bearing and in tumor-free mice (Figure 18) and the serum concentration of the ADC over time was as expected. Importantly, the PK of the ADC concentration in the serum correlated with the kinetics of antitumor efficacy observed in this xenograft model.

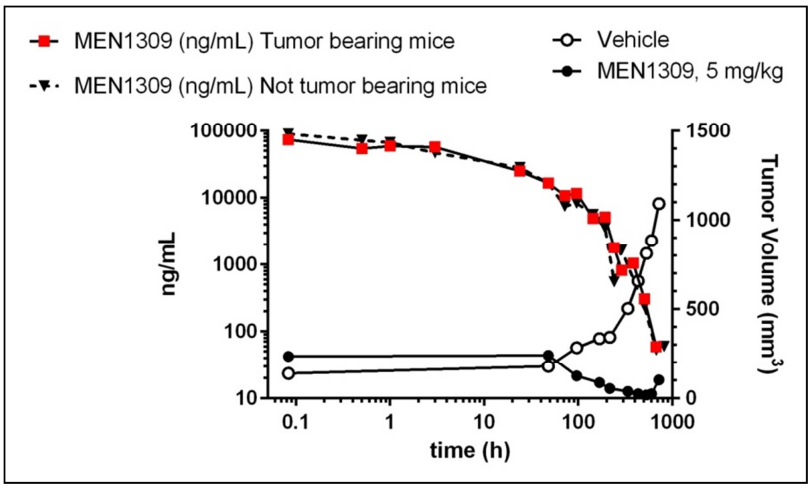

Figure 18. MEN1309/OBT076 PK profiling. Serum concentration versus time profile of MEN1309/OBT076 in tumor bearing (red square), and non-tumor bearing mice (black triangle) associated with the antitumor activity of MEN1309/OBT076 on HPAFII human pancreatic carcinoma xenograft model: open circle, tumor growth in the vehicle, and black circle in MEN1309/OBT076 treated mice.

By immunofluorescence (IF) labeling of phospho-histone H3, a significant anti-mitotic effect of the ADC was observed (Figure 19A-B). The fluorescent-positive cells (indicative of mitotic arrest) increased in the tumor mass in parallel with the reduction of tumor growth and correlated with the serum concentration of MEN1309/OBT076. A maximum level of phosphorylated H3 in tumor cells mass was obtained 96 hours after MEN1309/OBT076 administration.

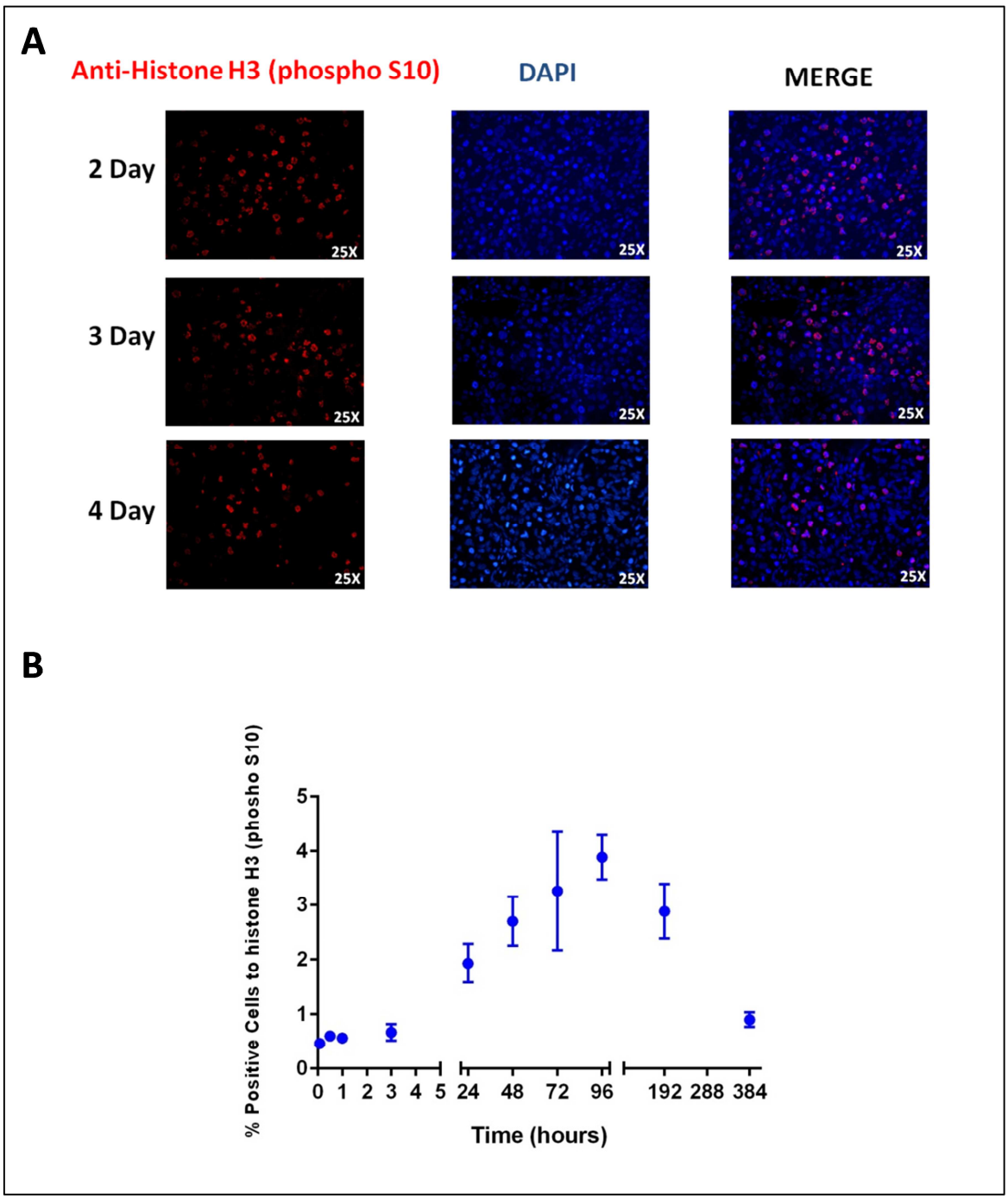

Figure 19. Pharmacodynamic activity. A) IF labeling of HPAFII human pancreatic tumor sections at different time points after MEN1309/OBT076 treatment. Alexa 594 (Red) nuclear histone H3 phosphorylated on serine10 (H3pS10); DAPI nuclear labeling (Blue); Merge. B) Percentage of Histone H3pS10 positive cells in HPAFII tumor sections versus time post-treatment with MEN1309/OBT076.

4.7 Antitumor activity of MEN1309/OBT076 fractionated dose in HPAFII xenograft model

In order to investigate whether fractionated dosing of MEN1309/OBT076 might have an impact on efficacy, the in-vivo antitumor activity of the ADC was explored in human pancreatic adenocarcinoma HPAFII xenograft model, expressing the antigen CD205 at a very high level. The efficacy of the single dose of MEN1309 at 5 mg/kg was compared to the following fractionated doses: 2,5 mg/kg with a q14dx2 schedule, and 1.6 mg/kg with a q7dx3 schedule. A single dose of MEN1309 at 5 mg/Kg induced a long lasting antitumor activity, confirming previously showed data (Figure 14A). At the end of the study the TVI was 66,8% (TVI at Nadir was 95.39%; Figure 20 B), and according to mRECIST criteria, evaluated at one week after the last treatment, three out of five mice showed a complete response (Figure 20 C). The intermediate MEN1309 dose, evaluated at the end of the study, showed a 40.5% TVI (TVI at Nadir was 77.20%; Figure 20 B), and according to mRECIST criteria, at one week after the last administration, two mice had a stable disease and three had a progressive disease (Figure 20C). The lowest dose of MEN1309 evaluated at the end of the study, showed 35,6% TVI (TVI at Nadir was 85.59%; Figure 20 B) better than the intermediate dosage, but a shorter time to re-growth compared to the single dose. Analysis, using the mRECIST criteria, evaluated at one week after the last treatment, showed that only one mouse had partial response, two mice had a stable disease and two mice had a progressive disease (Figure 20 C). All schedules were well tolerated with no

observed gross toxicities (e.g. body weight change, clinical signs and death events) in any treated mouse.

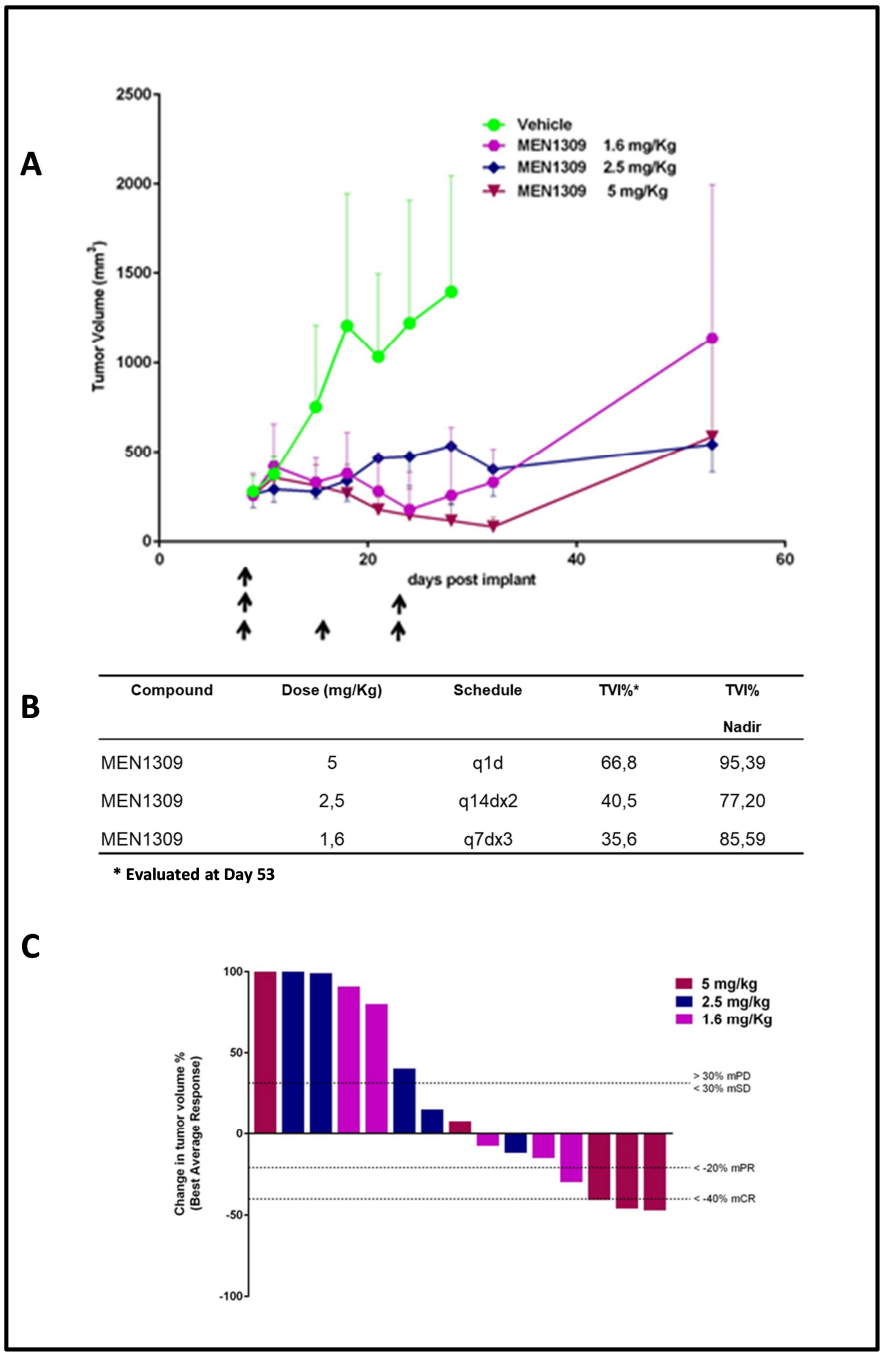

Compound	Dose (mg/Kg)	Schedule	TVI%*	TVI% Nadir
MEN1309	5	q1d	66,8	95,39
MEN1309	2,5	q14dx2	40,5	77,20
MEN1309	1,6	q7dx3	35,6	85,59

*** Evaluated at Day 53**

Figure 20. MEN1309/OBT076 antitumor activity with fractionated dose. Antitumor efficacy of fractionated dose against the human pancreatic adenocarcinoma HPAFII tumor cell line HPAFII. A: Tumor growth; B: Tumor Volume Inhibition (TVI%) and C: waterfall plot. According to mRECIST criteria, response was evaluated one week after the last treatment. Each bar represents a single mouse: mCR Complete Response; mPR, Partial Response; mSD, Stable Disease; mPD, Progressive Disease.

5. Discussion

An increasing number of ADCs in clinical development highlights the interest in this type of targeted therapy, which exploits the specificity of tumor-associated antigens to distribute potent cytotoxic agents to solid and haematological tumors. In this thesis, we present the preclinical antitumor profile of the first-in-class ADC, MEN1309/OBT076, targeting tumors expressing the CD205 antigen. The payload DM4 is a maytansine derivative endowed with potent antimitotic effects due to its ability to inhibit microtubule assembly at nanomolar concentrations [79, 80]. The CD205 antigen, a transmembrane protein member of the macrophage mannose receptor family of C-type lectins, is an ideal target for an ADC based therapy since it is highly overexpressed in different solid tumors compared to healthy tissues. Antigen positivity observed in dendritic cells is not hypothesized to have a major impact on their potential antitumor immunity activity, due to the suggested non-endocytic function of CD205 expressed on mature dendritic cells [69]. Moreover, based on their low proliferation index, they should be spared by the cell killing activity exerted by the maytansinoid derivate payload. In addition, CD205 exhibits a rapid internalization rate, which allows the efficient delivery of the cytotoxic payload into the target cells. Consistent with the reported kinetics of other antigen/antibody complexes [81-83] and based on our data, the internalization rate seems to correlate with the expression levels of the antigen.

The only ADC approved for use in solid tumors, T-DM1 (Kadcycla), was developed from the therapeutic monoclonal antibody Trastuzumab (Herceptin), and in addition to the anti-mitotic activity of the payload, retain the mechanisms of action of Trastuzumab: 1) inhibition of HER-2 signaling; 2) Fcγ receptor mediated engagement of immune cells, which results in antibody-dependent cellular cytotoxicity (ADCC) [84]. Although MEN1309/OBT076 binds to the FcγRIIIA receptor, it was unable to mount the

mechanisms of ADCC and CDC. This might be related to the fast antigen/antibody complex internalization rate observed (a remarkable amount of re-localized antibody was already detected after 30 minutes of cells labeling), suggesting that the antibody is not bound to the membrane long enough to mount a detectable ADCC or CDC activity in a cell-based assay which lasts hours. However, the contribution of the immune activation functions, in terms of cell killing, would be quite limited compared to the cytotoxic potential mediated by the ADC payload.

We have shown that the conjugation of MBH1309/OBT076 with the DM4 toxin through a cleavable SPDB linker is the most effective construct in terms of antitumor activity [73]. In fact, the conjugation of DM1 through a non-cleavable linker was less active in tumors with a heterogeneous expression of the antigen. The cleavable linker allows the bystander-killing effect to eliminate antigen negative tumor cells [85]. Indeed, MEN1309/OBT076 demonstrated a cytotoxic activity in the picomolar range against cells having strong (IHC score of 3+) asc well as weak (IHC score of 1+) antigen expression. A negligible effect was observed on CD205 antigen negative cells, thus highlighting the specificity of this ADC.

At the preclinical level, MEN1309/OBT076 showed a remarkable antitumor activity in a panel of tumor xenografts and PDX models of TNBC.

Interestingly, in two xenograft models of TNBC expressing low CD205 antigen (weak staining with 1+ IHC score), 2.5 mg/Kg of MEN1309/OBT076 completely inhibited the tumor growth. A compelling in vivo efficacy was also observed on TNBC PDX models expressing the antigen at high levels. Furthermore, 5mg/kg of MEN1309/OBT076 also induced complete responses in the HPAFII pancreatic cancer xenograft model.

Treatment of the low antigen expressing SW780 bladder cancer xenograft model with MEN1309/OBT076 produced a good response, whereas the efficacy was reduced when we treated the bladder PDX models expressing intermediate antigen levels.

Overall, comparing the activity of MEN1309/OBT076 in TNBC to that in pancreatic cancer, suggests that the antigen expression level is not the sole factor contributing to the ADC-mediated tumor cell cytotoxicity; the sensitivity of the tumor histotype to the toxin, the internalization rate and the cellular metabolism, appear to play important roles in the antitumor efficacy of the compound. As a whole, these data suggest that the antigen expression is necessary but not sufficient for significant antitumor activity of MEN1309/OBT076.

The PK/PD experiment conducted on the HPAFII pancreatic xenograft model indicates that the serum concentration of MEN1309/OBT076 positively correlates with the tumor growth inhibition observed. Interestingly, no difference was found between the MEN1309/OBT076 serum PK profile in tumor bearing and non-tumor bearing mice, suggesting that tumor cells highly expressing CD205 do not act as a substantial sink for the ADC. These PK data are similar to that seen for other ADCs [86]. The time course of histone H3 phosphorylation (a PD marker of DM4 activity) in the HPAFII tumor mass showed a significant gradual increase of mitotically arrested cells up to 96 hours after MEN1309/OBT076 administration. Importantly, the onset of the antitumor effect was concurrent with the peak of histone H3 phosphorylation.

In addition, the exploration of dosing schedule might contribute to the understanding and selection of a rationale dosing schedule for clinical assessment. Thus, a common approch that may have an impact on efficacy and to improve tolerability of ADCs with narrow

therapeutic window [87], is the fractioning of the dose, maintaining the total amount of compound adminestered.

For this purpose, we tested two fractionated dosing schedules (q7dx3 at 1.6 mg/kg and q14dx2 at 2.5mg/kg) compare to fully dosage of 5 mg/Kg with a q21dx3 schedule. The results showed the fully dosage performed better than the two different schedules and dosages.

Furthermore, non-clinical studies to characterize the pharmacokinetics (PK) and assess the safety profile of MEN1309/OBT076 were performed in Cynomolgus Monkeys, selected as the pharmacologically the relevant species, since MEN1309/OBT076 cross-reacts only with the cynomolgus antigen. These studies demonstrated that the antibody exhibits appropriate PK parameters with an acceptable toxicity profile and strongly support the clinical development of MEN1309/OBT076.

We acknowledge that the use of in-vitro and in-vivo models has limitations when characterizing ADC. In particular, we are aware that the cancer cell lines and PDX models deployed in this study are only minimally representative of a clinically relevant patient population in terms of tumor heterogeneity and sample size. Moreover, the use of immunocompromised mice as recipients of human-derived tumors prevents assessing the impact of the human immune system on ADC efficacy and toxicity.

Overall, the data presented here demonstrate that MEN1309/OBT076 is a selective and promising first-in-class antitumor ADC with an acceptable toxicity profile in relevant preclinical species. These data supported the start of the first-in-human SHUTTLE study (NCT03403725) in CD205-positive metastatic solid tumors and relapsed or refractory non-Hodgkin’s lymphoma patients.

6. Bibliography

1. Lambert, J.M., *Antibody-Drug Conjugates (ADCs): Magic Bullets at Last!* Mol Pharm, 2015. **12**(6): p. 1701-2.
2. Silverstein, A.M., *The collected papers of Paul Ehrlich : why was volume 4 never published?* Bull Hist Med, 2002. **76**(2): p. 335-9.
3. Schrama, D., R.A. Reisfeld, and J.C. Becker, *Antibody targeted drugs as cancer therapeutics.* Nat Rev Drug Discov, 2006. **5**(2): p. 147-59.
4. Diamantis, N. and U. Banerji, *Antibody-drug conjugates--an emerging class of cancer treatment.* Br J Cancer, 2016. **114**(4): p. 362-7.
5. Chari, R.V., M.L. Miller, and W.C. Widdison, *Antibody-drug conjugates: an emerging concept in cancer therapy.* Angew Chem Int Ed Engl, 2014. **53**(15): p. 3796-827.
6. Dan, N., et al., *Antibody-Drug Conjugates for Cancer Therapy: Chemistry to Clinical Implications.* Pharmaceuticals (Basel), 2018. **11**(2).
7. Carter, P.J. and P.D. Senter, *Antibody-drug conjugates for cancer therapy.* Cancer J, 2008. **14**(3): p. 154-69.
8. Kohler, G. and C. Milstein, *Continuous cultures of fused cells secreting antibody of predefined specificity.* Nature, 1975. **256**(5517): p. 495-7.
9. Lin, K. and J. Tibbitts, *Pharmacokinetic considerations for antibody drug conjugates.* Pharm Res, 2012. **29**(9): p. 2354-66.
10. Jiang, X.R., et al., *Advances in the assessment and control of the effector functions of therapeutic antibodies.* Nat Rev Drug Discov, 2011. **10**(2): p. 101-11.
11. Salfeld, J.G., *Isotype selection in antibody engineering.* Nat Biotechnol, 2007. **25**(12): p. 1369-72.
12. Beck, A., et al., *Strategies and challenges for the next generation of antibody-drug conjugates.* Nat Rev Drug Discov, 2017. **16**(5): p. 315-337.
13. Bargh, J.D., et al., *Cleavable linkers in antibody-drug conjugates.* Chem Soc Rev, 2019. **48**(16): p. 4361-4374.
14. Tang, H., et al., *The Analysis of Key Factors Related to ADCs Structural Design.* Front Pharmacol, 2019. **10**: p. 373.
15. Kellogg, B.A., et al., *Disulfide-linked antibody-maytansinoid conjugates: optimization of in vivo activity by varying the steric hindrance at carbon atoms adjacent to the disulfide linkage.* Bioconjug Chem, 2011. **22**(4): p. 717-27.
16. Golfier, S., et al., *Anetumab ravtansine: a novel mesothelin-targeting antibody-drug conjugate cures tumors with heterogeneous target expression favored by bystander effect.* Mol Cancer Ther, 2014. **13**(6): p. 1537-48.
17. Staudacher, A.H. and M.P. Brown, *Antibody drug conjugates and bystander killing: is antigen-dependent internalisation required?* Br J Cancer, 2017. **117**(12): p. 1736-1742.
18. Erickson, H.K., et al., *Tumor delivery and in vivo processing of disulfide-linked and thioether-linked antibody-maytansinoid conjugates.* Bioconjug Chem, 2010. **21**(1): p. 84-92.
19. Bernardes, G.J., et al., *A traceless vascular-targeting antibody-drug conjugate for cancer therapy.* Angew Chem Int Ed Engl, 2012. **51**(4): p. 941-4.
20. Tsuchikama, K. and Z. An, *Antibody-drug conjugates: recent advances in conjugation and linker chemistries.* Protein Cell, 2018. **9**(1): p. 33-46.
21. Sun, X., et al., *Design of antibody-maytansinoid conjugates allows for efficient detoxification via liver metabolism.* Bioconjug Chem, 2011. **22**(4): p. 728-35.

22. Erickson, H.K., et al., *The effect of different linkers on target cell catabolism and pharmacokinetics/pharmacodynamics of trastuzumab maytansinoid conjugates.* Mol Cancer Ther, 2012. **11**(5): p. 1133-42.
23. Shor, B., H.P. Gerber, and P. Sapra, *Preclinical and clinical development of inotuzumab-ozogamicin in hematological malignancies.* Mol Immunol, 2015. **67**(2 Pt A): p. 107-16.
24. Gupta, P.B., C.L. Chaffer, and R.A. Weinberg, *Cancer stem cells: mirage or reality?* Nat Med, 2009. **15**(9): p. 1010-2.
25. Ichimura, M., et al., *Duocarmycins, new antitumor antibiotics produced by Streptomyces; producing organisms and improved production.* J Antibiot (Tokyo), 1991. **44**(10): p. 1045-53.
26. Mantaj, J., et al., *From Anthramycin to Pyrrolobenzodiazepine (PBD)-Containing Antibody-Drug Conjugates (ADCs).* Angew Chem Int Ed Engl, 2017. **56**(2): p. 462-488.
27. Li, W., et al., *Biosynthesis of sibiromycin, a potent antitumor antibiotic.* Appl Environ Microbiol, 2009. **75**(9): p. 2869-78.
28. Bouchard, H., C. Viskov, and C. Garcia-Echeverria, *Antibody-drug conjugates-a new wave of cancer drugs.* Bioorg Med Chem Lett, 2014. **24**(23): p. 5357-63.
29. Wall, M.E., et al., *Plant Antitumor Agents. I. The Isolation and Structure of Camptothecin, a Novel Alkaloidal Leukemia and Tumor Inhibitor from Camptotheca acuminata1,2.* Journal of the American Chemical Society, 1966. **88**(16): p. 3888-3890.
30. Hsiang, Y.H., et al., *Camptothecin induces protein-linked DNA breaks via mammalian DNA topoisomerase I.* J Biol Chem, 1985. **260**(27): p. 14873-8.
31. Polakis, P., *Antibody Drug Conjugates for Cancer Therapy.* Pharmacol Rev, 2016. **68**(1): p. 3-19.
32. Bai, R.L., G.R. Pettit, and E. Hamel, *Binding of dolastatin 10 to tubulin at a distinct site for peptide antimitotic agents near the exchangeable nucleotide and vinca alkaloid sites.* J Biol Chem, 1990. **265**(28): p. 17141-9.
33. Li, F., et al., *Intracellular Released Payload Influences Potency and Bystander-Killing Effects of Antibody-Drug Conjugates in Preclinical Models.* Cancer Res, 2016. **76**(9): p. 2710-9.
34. Lambert, J.M. and R.V. Chari, *Ado-trastuzumab Emtansine (T-DM1): an antibody-drug conjugate (ADC) for HER2-positive breast cancer.* J Med Chem, 2014. **57**(16): p. 6949-64.
35. Issell, B.F. and S.T. Crooke, *Maytansine.* Cancer Treat Rev, 1978. **5**(4): p. 199-207.
36. Adem, Y.T., et al., *Auristatin antibody drug conjugate physical instability and the role of drug payload.* Bioconjug Chem, 2014. **25**(4): p. 656-64.
37. Moussa, E.M., et al., *Immunogenicity of Therapeutic Protein Aggregates.* J Pharm Sci, 2016. **105**(2): p. 417-430.
38. Hamblett, K.J., et al., *Effects of drug loading on the antitumor activity of a monoclonal antibody drug conjugate.* Clin Cancer Res, 2004. **10**(20): p. 7063-70.
39. McDonagh, C.F., et al., *Engineered antibody-drug conjugates with defined sites and stoichiometries of drug attachment.* Protein Eng Des Sel, 2006. **19**(7): p. 299-307.
40. Hoffmann, R.M., et al., *Antibody structure and engineering considerations for the design and function of Antibody Drug Conjugates (ADCs).* Oncoimmunology, 2018. **7**(3): p. e1395127.

41. Junutula, J.R., et al., *Site-specific conjugation of a cytotoxic drug to an antibody improves the therapeutic index.* Nat Biotechnol, 2008. **26**(8): p. 925-32.
42. Axup, J.Y., et al., *Synthesis of site-specific antibody-drug conjugates using unnatural amino acids.* Proc Natl Acad Sci U S A, 2012. **109**(40): p. 16101-6.
43. Jeger, S., et al., *Site-specific and stoichiometric modification of antibodies by bacterial transglutaminase.* Angew Chem Int Ed Engl, 2010. **49**(51): p. 9995-7.
44. Kamath, A.V. and S. Iyer, *Preclinical Pharmacokinetic Considerations for the Development of Antibody Drug Conjugates.* Pharm Res, 2015. **32**(11): p. 3470-9.
45. Epenetos, A.A., et al., *Limitations of radiolabeled monoclonal antibodies for localization of human neoplasms.* Cancer Res, 1986. **46**(6): p. 3183-91.
46. Leu, A.J., et al., *Absence of functional lymphatics within a murine sarcoma: a molecular and functional evaluation.* Cancer Res, 2000. **60**(16): p. 4324-7.
47. Heldin, C.H., et al., *High interstitial fluid pressure - an obstacle in cancer therapy.* Nat Rev Cancer, 2004. **4**(10): p. 806-13.
48. Jain, R.K., *Barriers to drug delivery in solid tumors.* Sci Am, 1994. **271**(1): p. 58-65.
49. Pastuskovas, C.V., et al., *Effect of immune complex formation on the distribution of a novel antibody to the ovarian tumor antigen CA125.* Drug Metab Dispos, 2010. **38**(12): p. 2309-19.
50. Deng, R., et al., *Monoclonal antibodies: what are the pharmacokinetic and pharmacodynamic considerations for drug development?* Expert Opin Drug Metab Toxicol, 2012. **8**(2): p. 141-60.
51. Bross, P.F., et al., *Approval summary: gemtuzumab ozogamicin in relapsed acute myeloid leukemia.* Clin Cancer Res, 2001. **7**(6): p. 1490-6.
52. Walter, R.B., et al., *Acute myeloid leukemia stem cells and CD33-targeted immunotherapy.* Blood, 2012. **119**(26): p. 6198-208.
53. Walter, R.B., et al., *CD33 expression and P-glycoprotein-mediated drug efflux inversely correlate and predict clinical outcome in patients with acute myeloid leukemia treated with gemtuzumab ozogamicin monotherapy.* Blood, 2007. **109**(10): p. 4168-70.
54. van Der Velden, V.H., et al., *Targeting of the CD33-calicheamicin immunoconjugate Mylotarg (CMA-676) in acute myeloid leukemia: in vivo and in vitro saturation and internalization by leukemic and normal myeloid cells.* Blood, 2001. **97**(10): p. 3197-204.
55. Polakis, P., *Arming antibodies for cancer therapy.* Curr Opin Pharmacol, 2005. **5**(4): p. 382-7.
56. Senter, P.D. and E.L. Sievers, *The discovery and development of brentuximab vedotin for use in relapsed Hodgkin lymphoma and systemic anaplastic large cell lymphoma.* Nat Biotechnol, 2012. **30**(7): p. 631-7.
57. Moasser, M.M., *The oncogene HER2: its signaling and transforming functions and its role in human cancer pathogenesis.* Oncogene, 2007. **26**(45): p. 6469-87.
58. Yilmaz, M., S. Richard, and E. Jabbour, *The clinical potential of inotuzumab ozogamicin in relapsed and refractory acute lymphocytic leukemia.* Ther Adv Hematol, 2015. **6**(5): p. 253-61.
59. Piccaluga, P.P., et al., *Surface antigens analysis reveals significant expression of candidate targets for immunotherapy in adult acute lymphoid leukemia.* Leuk Lymphoma, 2011. **52**(2): p. 325-7.
60. Taylor, M.E., et al., *Primary structure of the mannose receptor contains multiple motifs resembling carbohydrate-recognition domains.* J Biol Chem, 1990. **265**(21): p. 12156-62.

61. Ezekowitz, R.A., et al., *Molecular characterization of the human macrophage mannose receptor: demonstration of multiple carbohydrate recognition-like domains and phagocytosis of yeasts in Cos-1 cells.* J Exp Med, 1990. **172**(6): p. 1785-94.
62. Zelensky, A.N. and J.E. Gready, *The C-type lectin-like domain superfamily.* Febs j, 2005. **272**(24): p. 6179-217.
63. East, L. and C.M. Isacke, *The mannose receptor family.* Biochim Biophys Acta, 2002. **1572**(2-3): p. 364-86.
64. Shrimpton, R.E., et al., *CD205 (DEC-205): a recognition receptor for apoptotic and necrotic self.* Mol Immunol, 2009. **46**(6): p. 1229-39.
65. Heath, W.R., et al., *Cross-presentation, dendritic cell subsets, and the generation of immunity to cellular antigens.* Immunol Rev, 2004. **199**: p. 9-26.
66. Jiang, W., et al., *The receptor DEC-205 expressed by dendritic cells and thymic epithelial cells is involved in antigen processing.* Nature, 1995. **375**(6527): p. 151-5.
67. Bonifaz, L., et al., *Efficient targeting of protein antigen to the dendritic cell receptor DEC-205 in the steady state leads to antigen presentation on major histocompatibility complex class I products and peripheral CD8+ T cell tolerance.* J Exp Med, 2002. **196**(12): p. 1627-38.
68. Mahnke, K., et al., *The dendritic cell receptor for endocytosis, DEC-205, can recycle and enhance antigen presentation via major histocompatibility complex class II-positive lysosomal compartments.* J Cell Biol, 2000. **151**(3): p. 673-84.
69. Butler, M., et al., *Altered expression and endocytic function of CD205 in human dendritic cells, and detection of a CD205-DCL-1 fusion protein upon dendritic cell maturation.* Immunology, 2007. **120**(3): p. 362-71.
70. Kato, M., et al., *Hodgkin's lymphoma cell lines express a fusion protein encoded by intergenically spliced mRNA for the multilectin receptor DEC-205 (CD205) and a novel C-type lectin receptor DCL-1.* J Biol Chem, 2003. **278**(36): p. 34035-41.
71. Giridhar, P.V., et al., *Interleukin-6 receptor enhances early colonization of the murine omentum by upregulation of a mannose family receptor, LY75, in ovarian tumor cells.* Clin Exp Metastasis, 2011. **28**(8): p. 887-97.
72. Faddaoui, A., et al., *The mannose receptor LY75 (DEC205/CD205) modulates cellular phenotype and metastatic potential of ovarian cancer cells.* Oncotarget, 2016. **7**(12): p. 14125-42.
73. Merlino, G., et al., *MEN1309/OBT076, a First-In-Class Antibody-Drug Conjugate Targeting CD205 in Solid Tumors.* Mol Cancer Ther, 2019. **18**(9): p. 1533-1543.
74. Massa, S., et al., *CD205, a target antigen for a novel ADC: Evaluation of antigen expression on TNBC, pancreatic adenocarcinoma and bladder urothelial carcinoma.* Journal of Clinical Oncology, 2019. **37**(15_suppl): p. e14726-e14726.
75. Workman, P., et al., *Guidelines for the welfare and use of animals in cancer research.* Br J Cancer, 2010. **102**(11): p. 1555-77.
76. Euhus, D.M., et al., *Tumor measurement in the nude mouse.* J Surg Oncol, 1986. **31**(4): p. 229-34.
77. Gao, H., et al., *High-throughput screening using patient-derived tumor xenografts to predict clinical trial drug response.* Nat Med, 2015. **21**(11): p. 1318-25.
78. Prigent, C. and S. Dimitrov, *Phosphorylation of serine 10 in histone H3, what for?* J Cell Sci, 2003. **116**(Pt 18): p. 3677-85.
79. Kupchan, S.M., et al., *Maytansine, a novel antileukemic ansa macrolide from Maytenus ovatus.* J Am Chem Soc, 1972. **94**(4): p. 1354-6.

80. Kupchan, S.M., et al., *The maytansinoids. Isolation, structural elucidation, and chemical interrelation of novel ansa macrolides.* J Org Chem, 1977. **42**(14): p. 2349-57.
81. Mazot, P., et al., *Internalization and down-regulation of the ALK receptor in neuroblastoma cell lines upon monoclonal antibodies treatment.* PLoS One, 2012. **7**(3): p. e33581.
82. Perera, R.M., et al., *Internalization, intracellular trafficking, and biodistribution of monoclonal antibody 806: a novel anti-epidermal growth factor receptor antibody.* Neoplasia, 2007. **9**(12): p. 1099-110.
83. Terp, M.G., et al., *Anti-human CD73 monoclonal antibody inhibits metastasis formation in human breast cancer by inducing clustering and internalization of CD73 expressed on the surface of cancer cells.* J Immunol, 2013. **191**(8): p. 4165-73.
84. Junttila, T.T., et al., *Trastuzumab-DM1 (T-DM1) retains all the mechanisms of action of trastuzumab and efficiently inhibits growth of lapatinib insensitive breast cancer.* Breast Cancer Res Treat, 2011. **128**(2): p. 347-56.
85. Ogitani, Y., et al., *Bystander killing effect of DS-8201a, a novel anti-human epidermal growth factor receptor 2 antibody-drug conjugate, in tumors with human epidermal growth factor receptor 2 heterogeneity.* Cancer Sci, 2016. **107**(7): p. 1039-46.
86. Leal, M., et al., *Preclinical Development of an anti-5T4 Antibody-Drug Conjugate: Pharmacokinetics in Mice, Rats, and NHP and Tumor/Tissue Distribution in Mice.* Bioconjug Chem, 2015. **26**(11): p. 2223-32.
87. Donaghy, H., *Effects of antibody, drug and linker on the preclinical and clinical toxicities of antibody-drug conjugates.* MAbs, 2016. **8**(4): p. 659-71.